Cell Death and Differentiation (2013) 20, 1631–1643

www.nature.com/cdd

Identification of PTEN at the ER and MAMs and its regulation of Ca^{2+} signaling and apoptosis in a protein phosphatase-dependent manner

A Bononi[1], M Bonora[1], S Marchi[1], S Missiroli[1], F Poletti[1], C Giorgi[1], PP Pandolfi[2] and P Pinton*[,1]

The tumor suppressor activity of PTEN (phosphatase and tensin homolog deleted on chromosome 10) is thought to be largely attributable to its lipid phosphatase activity. PTEN dephosphorylates the lipid second messenger phosphatidylinositol 3,4,5-trisphosphate to directly antagonize the phosphoinositide 3-kinase-Akt pathway and prevent the activating phosphorylation of Akt. PTEN has also other proposed mechanisms of action, including a poorly characterized protein phosphatase activity, protein–protein interactions, as well as emerging functions in different compartment of the cells such as nucleus and mitochondria. We show here that a fraction of PTEN protein localizes to the endoplasmic reticulum (ER) and mitochondria-associated membranes (MAMs), signaling domains involved in calcium ($^{2+}$) transfer from the ER to mitochondria and apoptosis induction. We demonstrate that PTEN silencing impairs ER Ca^{2+} release, lowers cytosolic and mitochondrial Ca^{2+} transients and decreases cellular sensitivity to Ca^{2+}-mediated apoptotic stimulation. Specific targeting of PTEN to the ER is sufficient to enhance ER-to-mitochondria Ca^{2+} transfer and sensitivity to apoptosis. PTEN localization at the ER is further increased during Ca^{2+}-dependent apoptosis induction. Importantly, PTEN interacts with the inositol 1,4,5-trisphosphate receptors (IP3Rs) and this correlates with the reduction in their phosphorylation and increased Ca^{2+} release. We propose that ER-localized PTEN regulates Ca^{2+} release from the ER in a protein phosphatase-dependent manner that counteracts Akt-mediated reduction in Ca^{2+} release via IP3Rs. These findings provide new insights into the mechanisms and the extent of PTEN tumor-suppressive functions, highlighting new potential strategies for therapeutic intervention.
Cell Death and Differentiation (2013) **20,** 1631–1643; doi:10.1038/cdd.2013.77; published online 28 June 2013

Phosphatase and tensin homolog deleted on chromosome 10 (PTEN) is among the most commonly lost or mutated tumor suppressors in human cancers,[1] and germline mutations of PTEN have been found in cancer predisposition syndromes.[2]

PTEN is a phosphatase that has both a lipid[3] and a dual-specificity protein phosphatase activity.[4] Its growth-attenuating activity has mostly been ascribed to the dephosphorylation of plasma membrane-localized phosphatidylinositol 3,4,5-trisphosphate (PIP3). Through this lipid phosphatase activity, PTEN keeps the levels of PIP3 low and antagonizes the phosphoinositide 3-kinase (PI3K)-Akt pathway. Akt is recruited to the plasma membrane by binding of its pleckstrin homology domain to PIP3, and here Akt is activated by phosphorylation. Functional inactivation of PTEN leads to higher basal levels of PIP3[5] and consequent Akt hyperactivation, which promotes cell growth, proliferation, survival and other cellular processes.[6]

Emerging evidence demonstrates that additional PTEN-dependent mechanisms are implicated in the regulation of cellular invasion, gene expression and tumor suppression. These include a poorly characterized protein phosphatase activity and proposed nonenzymatic mechanisms such as interaction with other proteins.[7–9] Recent advances have also proved the importance of PTEN subcellular localization. Localized PTEN activity appears to establish PIP3 signal gradients that regulate cell polarity during motility.[10] In addition, nuclear PTEN has important tumor-suppressive functions,[11,12] and mitochondrially localized PTEN contributes to mitochondria-dependent apoptosis under certain circumstances.[13,14]

Mitochondria and endoplasmic reticulum (ER) have emerged as cellular targets of oncogenes and tumor suppressors, as they are crucial nodes where significant remodeling of calcium (Ca^{2+}) signaling occurs in tumor cells to sustain proliferation and avoid cell death.[15,16] Indeed, despite controlling many processes essential for life, the ER-to-mitochondria Ca^{2+} transmission can be a potent death-inducing signal, as the enhancement of mitochondrial

[1]Department of Morphology, Surgery and Experimental Medicine, Section of General Pathology, Interdisciplinary Center for the Study of Inflammation (ICSI), Laboratory for Technologies of Advanced Therapies (LTTA), University of Ferrara, Ferrara, Italy and [2]Cancer Genetics Program, Beth Israel Deaconess Cancer Center, Departments of Medicine and Pathology, Beth Israel Deaconess Medical Center, Harvard Medical School, Boston, MA, USA
*Corresponding author: P Pinton, Department of Morphology, Surgery and Experimental Medicine, Section of General Pathology, Interdisciplinary Center for the Study of Inflammation (ICSI), Laboratory for Technologies of Advanced Therapies (LTTA), University of Ferrara, Via Luigi Borsari, 46, 44121 Ferrara, Italy.
Tel: +39 0532 455802; Fax: +39 0532 455351; E-mail: pnp@unife.it
Keywords: apoptosis; calcium; endoplasmic reticulum; mitochondria-associated membranes MAMs; mitochondria; PTEN
Abbreviations: ArA, arachidonic acid; $[Ca^{2+}]_c$, cytosolic $[Ca^{2+}]$; $[Ca^{2+}]_{er}$, endoplasmic reticulum $[Ca^{2+}]$; $[Ca^{2+}]_m$, mitochondrial $[Ca^{2+}]$; cytAEQ, cytosolic aequorin; ER, endoplasmic reticulum; erAEQ, endoplasmic reticulum-targeted mutated aequorin; ER-RFP, endoplasmic reticulum-targeted red fluorescent protein; GFP, green fluorescent protein; IP3R, inositol 1,4,5-trisphosphate receptor; MAMs, mitochondria-associated membranes; mtAEQ, mitochondria-targeted aequorin; mtDsRED, mitochondria-targeted red fluorescent protein; OMM, outer mitochondrial membrane; PI3K, phosphoinositide 3-kinase; PIP3, phosphatidylinositol 3,4,5-trisphosphate; PK, proteinase K; PTEN, phosphatase and tensin homolog deleted on chromosome 10; siRNA, small interfering RNA; XeC, xestospongin C
Received 24.8.12; revised 30.4.13; accepted 09.5.13; Edited by L Scorrano; published online 28.6.13

Ca^{2+} uptake generally correlates with increased sensitivity to apoptosis. The ER supplies Ca^{2+} directly to mitochondria via inositol 1,4,5-trisphosphate receptors (IP3Rs) at close contacts between the two organelles, referred to as mitochondria-associated membranes (MAMs). Ca^{2+}-handling proteins of both organelles are highly compartmentalized at MAMs, providing a direct and proper mitochondrial Ca^{2+} signaling. Recently, numerous other proteins have been characterized at MAMs, underlying the importance of this subcellular domain for signaling cell fate choices.[17]

Here, we provide unprecedented evidence that a fraction of cellular PTEN is localized at the ER and MAMs. We observed that during Ca^{2+}-dependent apoptosis the localization of PTEN to the ER further increase. At the ER, PTEN can interact with the type 3 IP3R (IP3R3), and this correlates with a decrease in Akt-mediated phosphorylation of the receptors and a subsequent increase in Ca^{2+} transfer from the ER to mitochondria. We found that PTEN exerts this function through its protein phosphatase activity. Collectively, our data reveal that, in addition to its canonical lipid phosphatase activity at the plasma membrane, a portion of ER-localized PTEN contributes to the regulation of ER-to-mitochondria Ca^{2+} transfer and apoptosis in a protein phosphatase-dependent manner. These findings support a novel mechanism of action of this important tumor suppressor.

Results

Besides the best known cytoplasmic and nuclear pools, it has been reported that PTEN can accumulate in mitochondria.

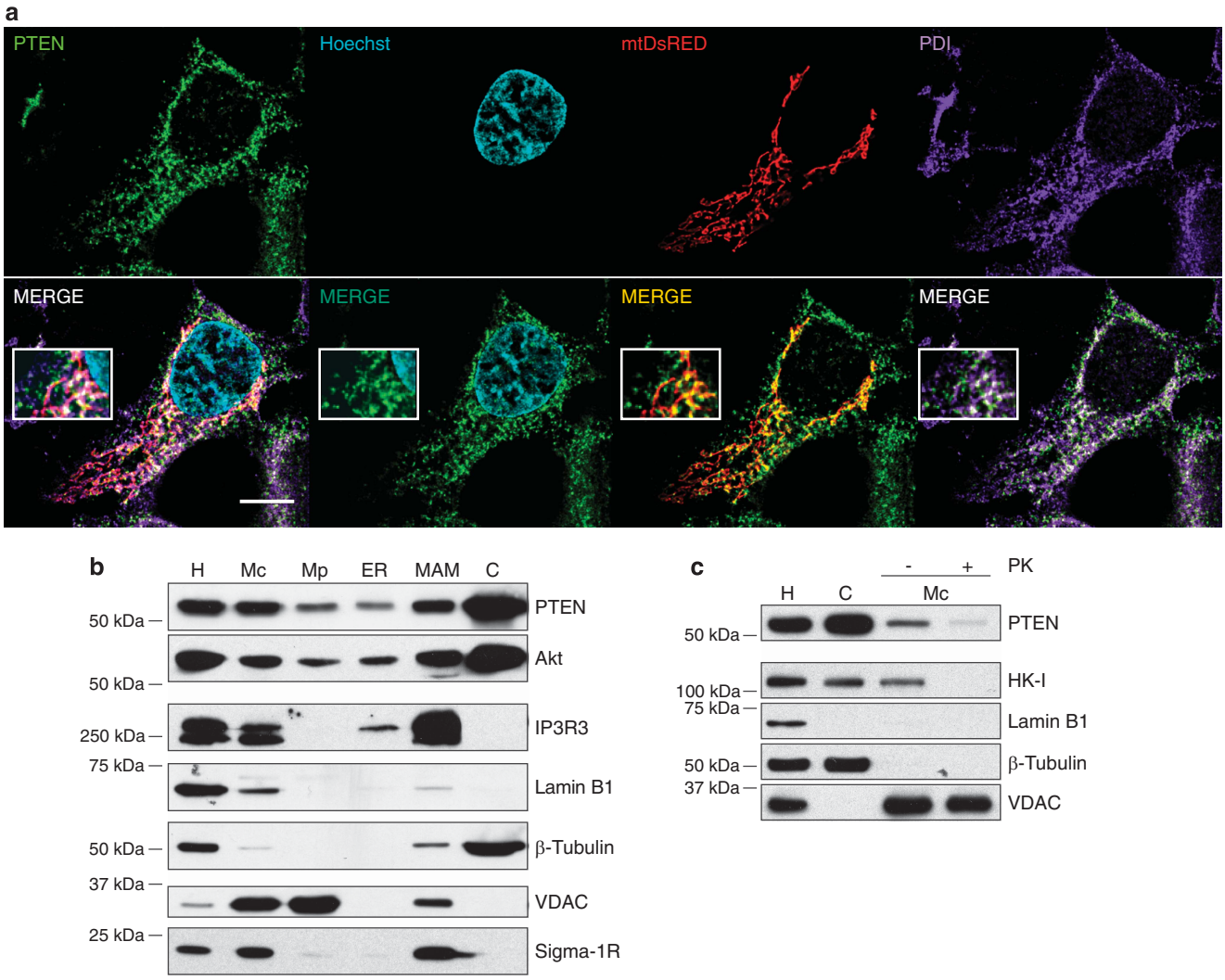

Figure 1 Subcellular localization of PTEN. (**a**) HEK-293 cells transfected with mtDsRED (mitochondria, red) were immunostained for PTEN (green), PDI (ER, blue) and loaded with Hoechst (nucleus, cyan). Merge images below show a succession of overlapping signals between: the four channels, PTEN and Hoechst, PTEN and mtDsRED, PTEN and PDI. Scale bar, 10 μm. Insets show magnified images. (**b**) Protein components of subcellular fractions prepared from HEK-293 cells revealed by western blot (WB) analysis. PTEN presence was shown using a specific monoclonal antibody. Akt presence was also verified in all fractions. Marker proteins indicate mitochondria (voltage-dependent anion channel, VDAC), ER (IP3R3), MAMs (Sigma-1R), cytosol (β-tubulin) and nucleus (lamin B1) (to exclude nuclear contamination). All markers were enriched in their respective compartments. The close apposition between ER and mitochondrial membranes at MAMs explained the presence of both VDAC and IP3R3 in these microdomains. H: homogenate; Mc: crude mitochondria; Mp: pure mitochondria; ER; MAM; and C: cytosol. (**c**) HEK-293 cells were subjected to subcellular fractionation. Mc fraction was further treated with PK, which can digest only those proteins that are not protected by closed phospholipidic bilayers. Hexokinase I (HK-I) was used as digestion control. Significant PK digestion of HK-I but not of VDAC was observed. The various fractions were immunoblotted with the indicated antibodies

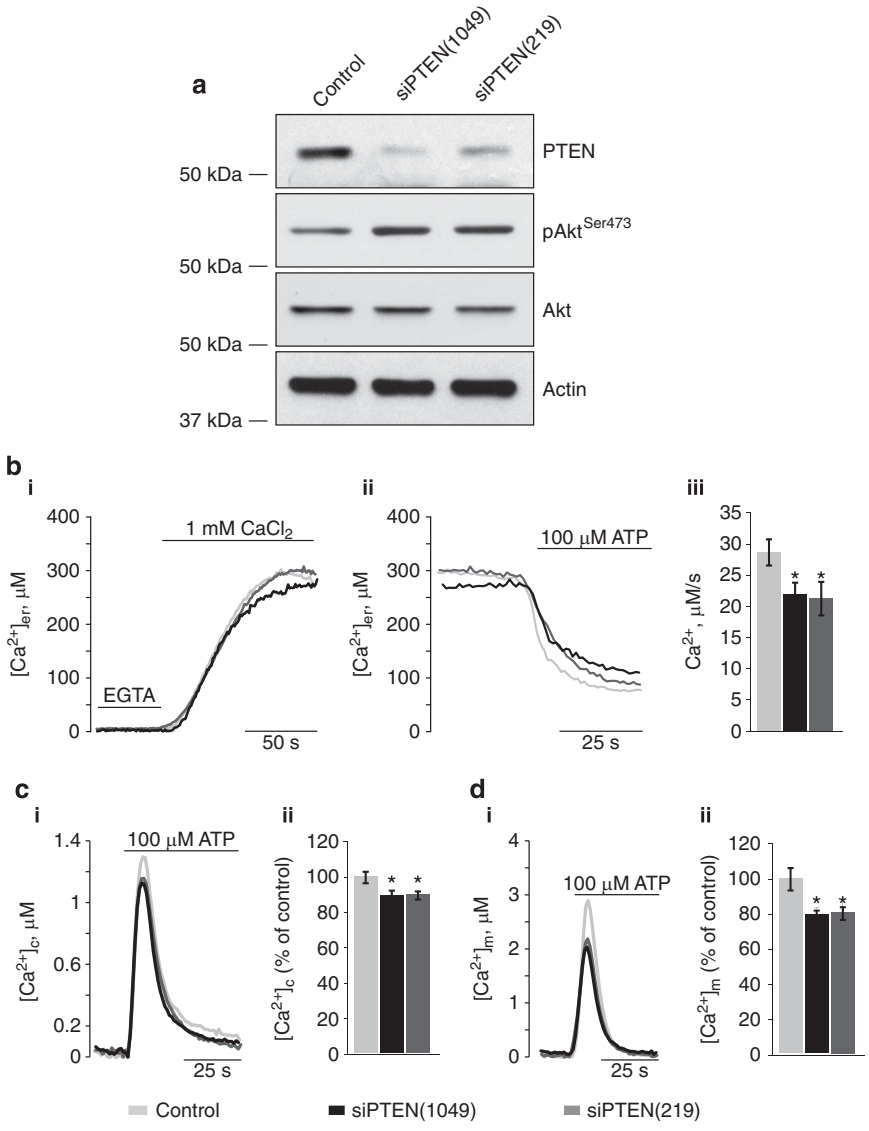

Figure 2 Effects of PTEN silencing on intracellular Ca^{2+} homeostasis. (**a**) Western blot of HEK-293 lysates from mock- (control) or siRNAs-PTEN-(siPTEN) transfected cells, probed for PTEN, $pAkt^{Ser473}$, total Akt and actin as loading control. (**b**) ER Ca^{2+} homeostasis. (**bi**) $[Ca^{2+}]_{er}$ steady-state levels (321.1 ± 27.30 μM for control $n = 10$; 286.7 ± 23.17 μM for siRNA-PTEN(1049) $n = 12$; 293.9 ± 27.59 μM for siRNA-PTEN(219) $n = 10$); (**bii**) modifications of ER Ca^{2+} release kinetics after PTEN silencing; (**biii**) mean rate of ER Ca^{2+} release (Vmax: 28.68 ± 2.12 μM/s for control $n = 10$; 21.89 ± 1.97 μM/s for siRNA-PTEN(1049) $n = 12$, $P < 0.05$; 21.25 ± 2.69 μM/s for siRNA-PTEN(219) $n = 10$, $P < 0.05$). Representative traces of (**ci**) $[Ca^{2+}]_c$ (peak values: 1.29 ± 0.04 μM for control $n = 31$; 1.15 ± 0.04 μM for siRNA-PTEN(1049) $n = 34$, $P < 0.05$; 1.16 ± 0.03 μM for siRNA-PTEN(219) $n = 34$, $P < 0.05$) and (**di**) mitochondrial Ca^{2+} transients ($[Ca^{2+}]_m$ peak values: 2.43 ± 0.15 μM for control $n = 14$; 1.94 ± 0.12 μM for siRNA-PTEN(1049) $n = 12$, $P < 0.05$; 1.97 ± 0.10 μM for siRNA-PTEN(219) $n = 13$, $P < 0.05$). Percent of $[Ca^{2+}]_c$ (**c–**ii) and $[Ca^{2+}]_m$ (**di**) peaks normalized to the mean of the control group. Mean ± S.E.M. of variation is shown as percentage. Cells were transfected and $[Ca^{2+}]$ was measured as described in Materials and Method. Where indicated, cells were challenged with 100 μM ATP to induce Ca^{2+} release from the ER. Traces and bar graphs are representatives of ≥10 samples from at least three independent experiments that yielded similar results. *$P < 0.05$

Here, we further investigate the intracellular localization of PTEN, in particular its presence in the ER, MAMs and mitochondria. To this end, we performed immunofluorescence (IF) and cell fractionation experiments (Figure 1). IF experiments revealed a typically diffuse, punctate staining pattern of PTEN that partially colocalizes in the ER, the mitochondrial network and the nucleus (Figure 1a). In parallel, we fractionated homogenates of HEK-293 cells (Figure 1b) and primary mouse embryonic fibroblasts (MEFs) (Supplementary Figure 1) by ultracentrifugation.[18] In addition to the cytosol, PTEN localized also to the mitochondria, ER and MAMs fractions. Akt was found in the same fractions.[19] To further discriminate whether PTEN associates with the outer mitochondrial membrane (OMM) or resides within these organelles, purified mitochondria were treated with proteinase K (PK). PTEN was almost completely degraded by PK treatment, indicating that it can associate with the OMM but not localize within mitochondria (Figure 1c).

In view of the localization of PTEN at the mitochondria, ER and MAMs, we investigated whether it has a role in regulating

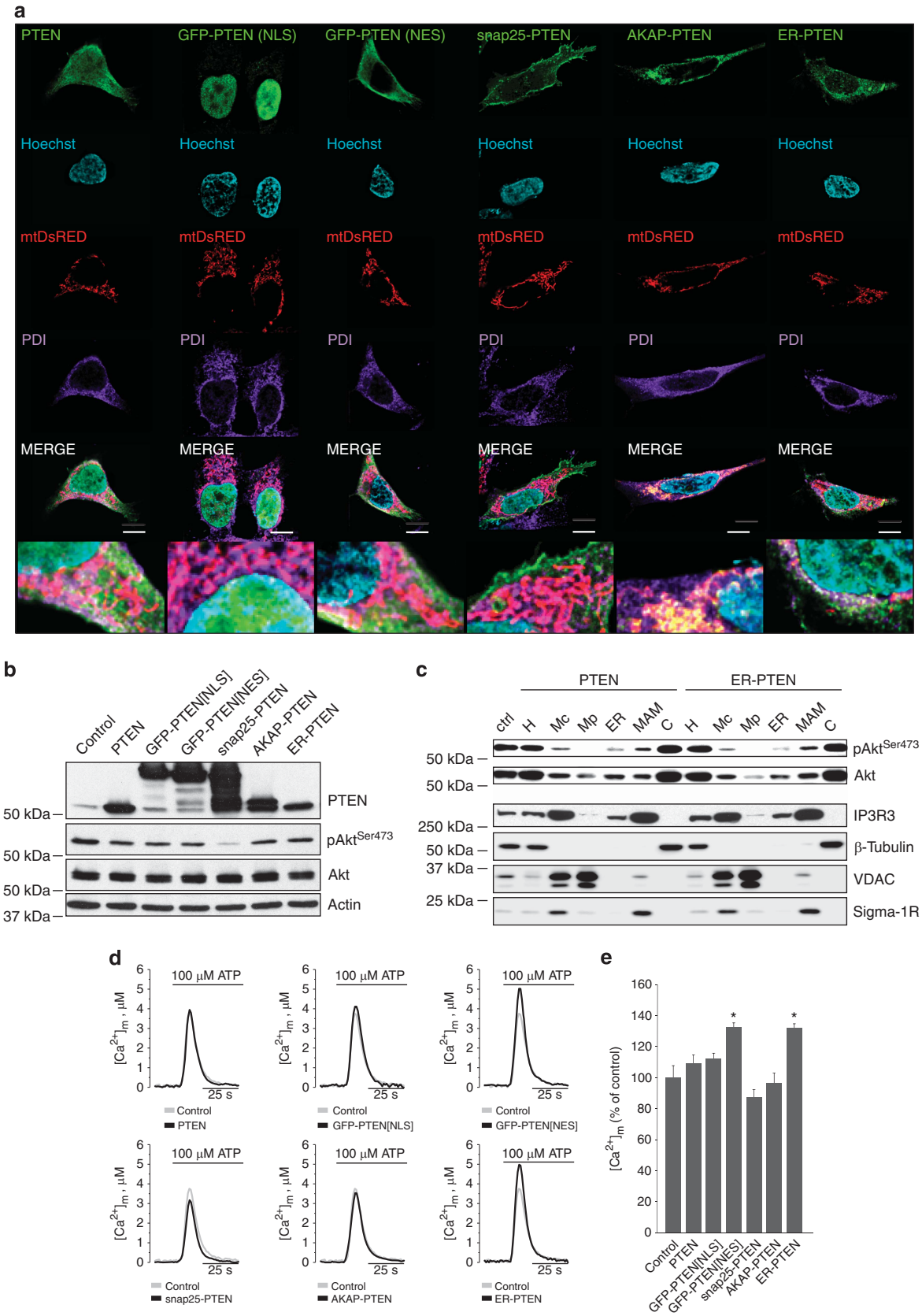
a
PTEN
GFP-PTEN (NLS)
GFP-PTEN (NES)
snap25-PTEN
AKAP-PTEN
ER-PTEN
Hoechst
mtDsRED
PDI
MERGE
b
Control
PTEN
GFP-PTEN[NLS]
GFP-PTEN[NES]
snap25-PTEN
AKAP-PTEN
ER-PTEN
50 kDa
pAkt^{Ser473}
Akt
Actin
37 kDa
c
PTEN
ER-PTEN
ctrl
H
Mc
Mp
ER
MAM
C
IP3R3
250 kDa
β-Tubulin
VDAC
Sigma-1R
25 kDa
d
100 μM ATP
$[Ca^{2+}]_m$, μM
25 s
Control
PTEN
GFP-PTEN[NLS]
GFP-PTEN[NES]
snap25-PTEN
AKAP-PTEN
ER-PTEN
e
$[Ca^{2+}]_m$ (% of control)

Ca^{2+} signaling between the two organelles. We first down-regulated PTEN expression by RNAi silencing (Figure 2). Two different small interfering RNAs (siRNAs), siRNA-PTEN(1049) and siRNA-PTEN(219), were generated and tested for specific silencing efficiency and the ability to increase the levels of activated, Ser473-phosphorylated, Akt ($pAkt^{Ser473}$). As expected, reduced levels of PTEN lead to increased Akt phosphorylation and activity (Figure 2a and Supplementary Figure 2a). We thus tested siRNAs-PTEN effect on intracellular Ca^{2+} homeostasis by co-transfecting them with specific organelle-targeted chimeras of the Ca^{2+}-sensitive photoprotein aequorin.[20] PTEN-silenced and control cells showed very similar loading kinetics and luminal ER Ca^{2+} concentrations ($[Ca^{2+}]_{er}$) at rest (Figures 2b–i). However, upon agonist stimulation with ATP, which acts on G_q-coupled plasma membrane receptors and causes the production of IP3, thus releasing Ca^{2+} from the ER to mitochondria, the release kinetics was slower in PTEN-silenced cells (Figure 2b–ii and iii), reflecting a slower flow of Ca^{2+} through the IP3Rs. In turn, ATP elicited significantly smaller $[Ca^{2+}]$ transients both in the cytosol ($[Ca^{2+}]_c$) (Figure 2c) and in the mitochondrial matrix ($[Ca^{2+}]_m$) (Figure 2d).

We further investigated whether a particular subcellular localization of PTEN could differentially affect mitochondrial Ca^{2+} handling, the main proximal target of Ca^{2+} signals arising from the ER. We compared the effects of over-expressed wild-type PTEN with chimeric PTEN proteins fused with nuclear localization signal (NLS) or nuclear export signal (NES) sequences designed to force nuclear (-NLS) or cytoplasmic (-NES) PTEN localization.[21] Further, we generated specific chimeric proteins that targeted the entire PTEN protein exclusively to the plasma membrane (snap25-PTEN), the OMM (AKAP-PTEN) or the cytoplasmic surface of the ER membrane (ER-PTEN). The intracellular localization of the different PTEN's chimeras is shown in Figure 3a. Figure 3b shows the expression levels of our set of constructs, as well as their ability to reduce $pAkt^{Ser473}$ levels in comparison with the control, with, remarkably, snap25-PTEN displaying the highest efficacy (Supplementary Figure 2b).

We then carried out mitochondrial Ca^{2+} measurements (Figures 3d and e). Upon agonist challenge, PTEN-overexpressing cells underwent a $[Ca^{2+}]_m$ rise comparable to control cells. Similar results were obtained upon overexpression of nuclear PTEN, whereas the $[Ca^{2+}]_m$ rise induced by the forced cytoplasmic PTEN chimera was markedly higher than in controls. These results prompted us to focus our attention on extranuclear compartments. We found that despite its maximum reduction in Akt phosphorylation and activity, $[Ca^{2+}]_m$ values of snap25-PTEN were comparable, if anything, slightly lower, to those of control cells. No differences in $[Ca^{2+}]_m$ peaks were observed between AKAP-PTEN-overexpressing and control cells, whereas in ER-PTEN-overexpressing cells the $[Ca^{2+}]_m$ transient was increased. Collectively, these data indicate that a subpopulation of cellular PTEN localized to the ER is specifically involved in the regulation of the agonist-induced Ca^{2+} fluxes from the ER to mitochondria. If all the different PTEN chimeras can reduce Akt phosphorylation, but only ER-targeted PTEN has the specific capability to increase mitochondrial Ca^{2+} uptake, we assumed that the $pAkt^{Ser473}$ pool relevant for the modulation of ER-to-mitochondria Ca^{2+} transfer should be restricted to the ER/MAMs fractions. To test this hypothesis, we fractionated PTEN- or ER-PTEN-overexpressing cells and analyzed Akt phosphorylation in the different cellular compartments (Figure 3c). A significant reduction in Akt activation ($pAkt^{Ser473}$/Akt ratio) was observed in the ER fraction of cells overexpressing ER-PTEN compared with PTEN. Akt activation was slightly lower also in the mitochondria and MAMs fractions of ER-PTEN-overexpressing cells and higher in the cytosol (Supplementary Figure 2c).

Ca^{2+} transfer from the ER to mitochondria has been implicated in multiple models of apoptosis as being directly responsible for mitochondrial Ca^{2+} overload, OMM permeabilization and caspase-mediated cell death.[15] Various apoptotic challenges, for example, C2-ceramide, oxidative stress (menadione, H_2O_2) or arachidonic acid (ArA), appear to induce the movement of Ca^{2+} from the ER to mitochondria, using Ca^{2+} as an apoptosis-sensitizing cofactor. We investigated whether PTEN silencing, overexpression or targeting to the ER differentially influences apoptotic signaling. Cells were loaded with the Ca^{2+} indicator Fura-2/AM and monitored during stimulation with ArA. Treatment with ArA triggers or enhances the release of Ca^{2+} from the ER, thus directly causing a small, transient $[Ca^{2+}]_c$ rise followed by a lower, sustained plateau.[22–24] After ArA treatment, we observed a rapid initial elevation of Fura-2-associated intracellular fluorescence, followed by progressive increase in intracellular Ca^{2+} over the next 15 min. The ArA-mediated increase of intracellular $[Ca^{2+}]$ was significantly depressed in cells preincubated with xestospongin C (XeC), a membrane-permeable antagonist of IP3Rs previously demonstrated to block IP3R-dependent Ca^{2+} release in various types of cells and tissues.[25] This suggests that IP3Rs are mostly specifically involved in ArA-induced Ca^{2+} release from the ER (Supplementary Figure 3a). We found that the cytosolic Ca^{2+} rise evoked by ArA is markedly blunted in PTEN-silenced cells (Figure 4ai and ii). Interestingly, the overexpression of ER-PTEN significantly increased the ArA-induced cytosolic Ca^{2+}

Figure 3 Subcellular targeting of PTEN differentially affects mitochondrial Ca^{2+} uptake. (**a**) Localization of recombinant wild-type PTEN and targeted PTEN chimeras in HEK-293 cells co-transfected with mtDsRED (mitochondria, red). Cells were immunostained for PTEN (green), PDI (ER, blue) and loaded with Hoechst (nucleus, cyan). Merge images show overlap between the four channels (white), and zoomed-in areas are below. Scale bars, 10 μm. (**b**) Western blot of HEK-293 lysates from mock-transfected cells (control) or cells overexpressing PTEN and targeted PTEN chimeras, probed for PTEN, $pAkt^{Ser473}$, total Akt and actin. (**c**) WB analysis of $pAkt^{Ser473}$ and total Akt levels from Percoll-purified subcellular fractions of HEK-293 cells transfected with recombinant wild-type PTEN or ER-PTEN. Untransfected cell homogenate (ctrl) was used as an indicator of Akt abundance and phosphorylation levels in physiological conditions. (**d**) Mitochondrial Ca^{2+} homeostasis modulation after PTEN, forced nuclear (NLS), cytoplasmic (NES), plasma membrane (snap25), OMM (AKAP) or ER chimeras overexpression (black) compared with control cells (gray); where indicated, cells were challenged with 100 μM ATP to induce Ca^{2+} release from the ER. (**e**) Percentage of $[Ca^{2+}]_m$ peaks normalized to the mean of the control group. Mean ± S.E.M. of variation is shown as percentage. Traces and bar graphs are representatives of $\geq$10 samples from at least three independent experiments that yielded similar results. *$P<0.05$

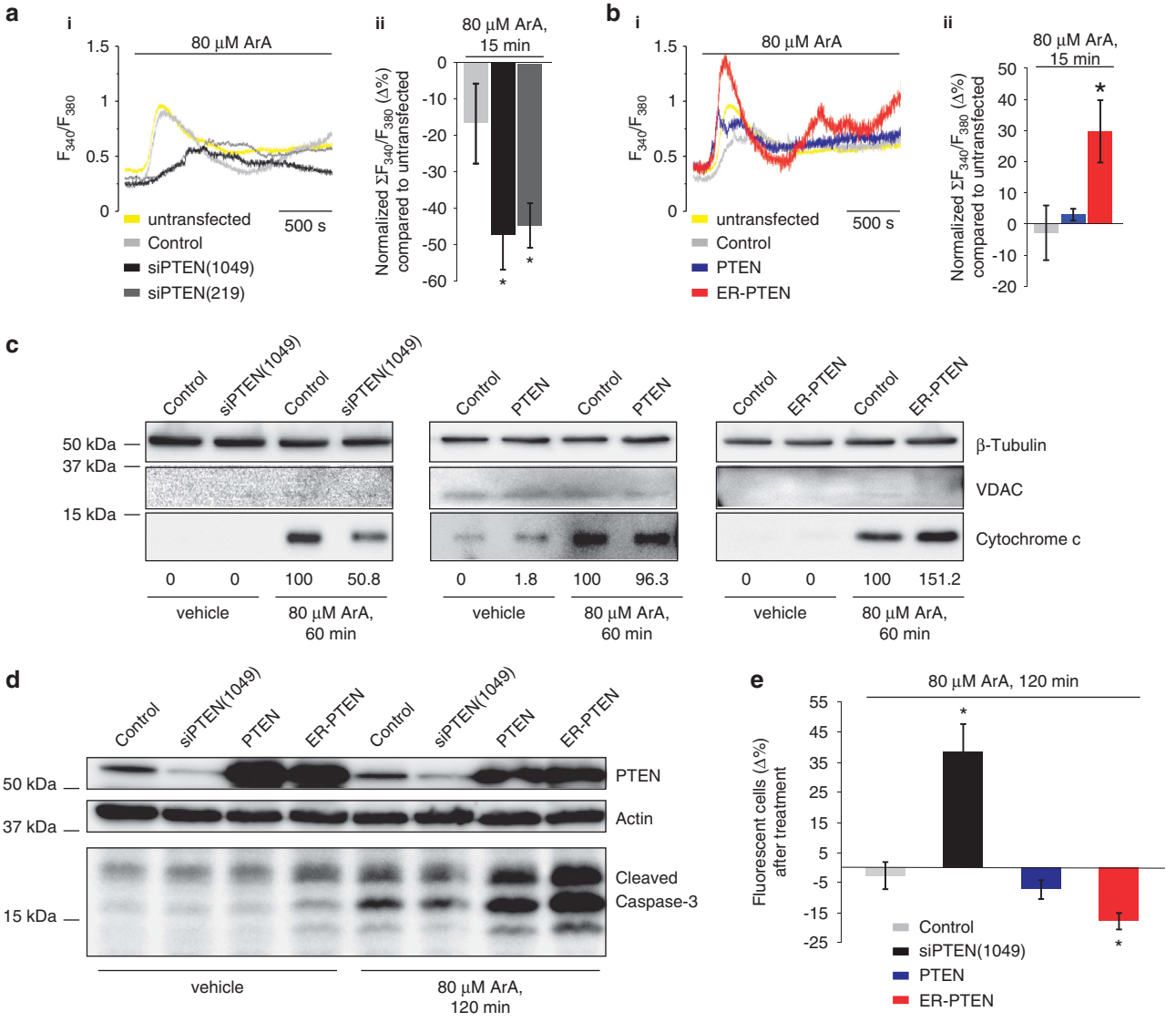

Figure 4 Effect of PTEN silencing, overexpression or targeting the outer surface of the ER on intracellular Ca^{2+} mobilization and apoptotic responses induced by ArA. (**a** and **b**) Cells were loaded with the Ca^{2+} indicator Fura-2/AM and untransfected cells in the same sample were used to compare changes in the 340/380 nm ratio. (**a**) Cytosolic Ca^{2+} increases induced by 80 μM ArA in PTEN-silenced cells, representative traces (i) and bars graphs (mean ± S.E.M.) (ii) showing the change in percentage of cytosolic Ca^{2+} increases normalized as $\Sigma(F_{340}/F_{380})$ over time in comparison with untransfected cells (Δ%: − 16.6 ± 11.0 for control $n = 58$ cells; − 47.4 ± 9.5 for siRNA-PTEN(1049) $n = 55$ cells, $P < 0.05$; − 44.8 ± 6.1 for siRNA-PTEN(219) $n = 59$ cells, $P < 0.05$). (**b**) Cytosolic Ca^{2+} increases induced by 80 μM ArA in cells overexpressing PTEN or ER-PTEN, representative traces (i) and bars graphs (mean ± S.E.M.) (ii) showing the change in percentage of cytosolic Ca^{2+} increases normalized as $\Sigma(F_{340}/F_{380})$ over time in comparison with untransfected cells (Δ%: − 2.8 ± 8.8 for control $n = 25$ cells; 3.1 ± 2.0 for PTEN $n = 24$ cells; 29.8 ± 10.0 for ER-PTEN $n = 36$ cells, $P < 0.05$). (**c**) HEK-293 cells were transfected with siPTEN(1049), PTEN, ER-PTEN or subjected to mock transfection (control). At 36 h post-transfection, cells were treated with 80 μM ArA or vehicle (EtOH) for 60 min, then cytosolic fractions were purified using a digitonin-based subcellular fractionation technique and analyzed by WB for the detection of cytosolic cytochrome *c*. As a loading control, β-tubulin was used for the cytosolic fraction, whereas the presence of the mitochondrial protein VDAC was assessed as an indicator of the purity of fractions. Representative results are reported. Numbers indicate densitometrically determined cytochrome *c* levels relative to β-tubulin. (**d**) HEK-293 cells transfected as in (**c**) were treated with 80 μM ArA or vehicle for 120 min, then total cell lysates were prepared and analyzed by WB to compare cleaved caspase-3 (17 kDa) levels. Results are from a single experiment that is representative of four separate experiments. (**e**) Sensitivity to apoptosis in cells co-transfected with a fluorescent marker and siPTEN(1049), PTEN or ER-PTEN. After treatment with 80 μM ArA or vehicle for 120 min, the survival of transfected and non-transfected cells was compared. In these experiments, mock-transfected and PTEN-overexpressing cells show no difference in the percentage of fluorescent cells after ArA treatment (Δ% − 2.5 ± 4.6 and − 7.1 ± 3.2, respectively); therefore they both have the same sensitivity to the apoptotic stimulus and die to the same extent. In the same conditions, an increase in the apparent transfection efficiency of PTEN-silenced cells was observed (Δ% 38.5 ± 9.4), indicating a decreased sensitivity to the apoptotic stimulus, whereas the reduced percentage of ER-PTEN-overexpressing fluorescent cells (Δ% − 17.6 ± 2.7) reflected a higher sensitivity to the apoptotic challenge. *$P < 0.05$

responses, whereas PTEN did not cause any differences (Figure 4bi and ii). We also ascertained the influence of Ca^{2+} mobilization from the ER on the increase of intracellular Ca^{2+} induced by ArA. We preformed the same experiment in conditions associated with extreme depletion of extracellular Ca^{2+}, and again we observed a significantly higher cytosolic Ca^{2+} response only in cells overexpressing ER-PTEN (Supplementary Figure 3b).

We then investigated whether the effects on Ca^{2+} mobilization of PTEN silencing, overexpression or targeting to the ER correlate with sensitivity to apoptosis. Western blot analysis revealed that the amount of cytochrome *c* released into the cytosol after ArA treatment was significantly reduced in PTEN-silenced cells and enhanced in ER-PTEN-transfected cells (Figure 3c). Accordingly, caspase-3 cleavage was reduced by the siRNA-mediated downregulation of PTEN and increased in ER-PTEN-overexpressing cells (Figure 4d and Supplementary Figure 3c). We observed no significant differences in PTEN-overexpressing cells. These results were also confirmed by counts of cell viability, revealing that PTEN-silenced cells were strongly protected from death, whereas ER-PTEN overexpression enhanced sensitivity to ArA (Figure 4e). Overall, these data indicate that the absence of PTEN causes a reduction in the amplitude of Ca^{2+} signals induced by apoptotic stimuli and protects from apoptosis, whereas ER-localized PTEN sensitizes cells to death by stimuli that require Ca^{2+} transfer from ER to mitochondria.

To gain insights into the mechanism by which PTEN localization at the ER may increase Ca^{2+} release via IP3Rs and sensitivity to apoptosis, we first sought to determine whether ER PTEN accumulation is a phenomenon related to Ca^{2+}-mediated apoptosis and its physiological significance. Cells were transfected with green fluorescent protein (GFP)-PTEN and the subcellular localization of the protein was followed after ArA treatment by imaging experiments. After 90 min of apoptotic challenge, we observed a substantial increase in GFP-PTEN colocalization with the ER marker ER-targeted red fluorescent protein, ER-RFP (Figure 5a, Supplementary Videos 1 and 2). We quantified the extent of PTEN overlapping the ER by calculating Manders' coefficients. After ArA treatment, the fraction of GFP-PTEN overlapping ER-RFP (Manders' green) was more than double, indicating a strong enrichment of PTEN to the ER (Figure 5a-ii). In contrast, no significant differences were observed in control GFP-transfected cells before and after ArA exposure (Figures 5a and 5a–iii; Supplementary video data, Supplementary Video 3). To independently confirm the increased localization of PTEN to the ER during Ca^{2+}-mediated apoptosis, we repeated the subcellular fractionation after ArA treatment (Figure 5b), and again detected an increased localization of PTEN to the ER fraction of apoptosing cells. Moreover, we observed a concomitant reduction of Akt presence in the mitochondrial, ER and MAMs fractions, and a reduction in Akt phosphorylation at the ER. ER accumulation was specific for PTEN, as the fractions were monitored for contamination using markers for the ER, cytosol, mitochondria and MAMs. Notably, in response to ArA, we observed a remarkable increase of VDAC at MAMs, according to previous studies demonstrating that under apoptosis-inducing conditions a narrowing of the ER-mitochondria associations occurs, and this is an important step in the execution of some apoptotic mechanisms.[26–29]

To investigate a possible mechanism for ER-PTEN action, we looked for a physical interaction between PTEN and IP3R3, as release of the ER Ca^{2+} through IP3R3 appears to sensitize cells to apoptotic stimuli.[24,30] We performed co-immunoprecipitation experiments of proteins extracted from the ER fraction in basal condition or after ArA treatment, and found that PTEN co-immunoprecipitated with IP3R3, together with Akt, a known iteractor and modulator of IP3R-mediated Ca^{2+} release from the ER.[19] Akt-dependent inhibition of Ca^{2+} transfer from the ER to mitochondria, through IP3R3 phosphorylation, protects from Ca^{2+}-mediated apoptosis.[24] The increased ER localization of PTEN in ArA-treated cells resulted in a greater amount of PTEN co-immunoprecipitating with IP3R3, but strikingly we observed a reduction of co-precipitated Akt. Moreover, the amount of phosphorylated-IP3R3 (pIP3R3) was lower in ArA-treated cells, as well as phosphorylated Akt ($pAkt^{Ser473}$) levels co-precipitated with IP3R3 (Figure 5c and Supplementary Figure 3d). These results suggested that when PTEN localized to the ER, Ca^{2+} flux through IP3R3 is strengthened by the inhibition of Akt activity.

Finally, we aimed to dissect the precise contribution of PTEN's different lipid and protein phosphatase activities in the regulation of Ca^{2+} signaling and apoptosis. We generated ER-targeted chimeras of the PTEN(C124S) mutant, which lacks both lipid and protein phosphatase activities[3] (ER-PTEN(C124S)), and of the PTEN(G129E) mutant, which displays a greatly reduced lipid phosphatase activity while retaining full protein phosphatase activity[31] (ER-PTEN (G129E)). ER-PTEN and ER-PTEN(G129E) had indistinguishable effects on Akt phosphorylation, whereas ER-PTEN(C124S) showed enhanced $pAkt^{Ser473}$ levels (Figure 6a and Supplementary Figure 4a). Ca^{2+} signals evoked by either agonist (Figure 6b) or ArA (Figure 6c and Supplementary Figure 4b) were comparable to ER-PTEN for ER-PTEN(G129E), whereas always lower for ER-PTEN(C124S). Consequently, in comparison with ER-PTEN(C124S), ER-PTEN(G129E) retained a greater capability to enhance cell death induced by ArA, as revealed by the higher amount of cytochrome *c* released into the cytosol (Figure 6d), increased caspase-3 cleavage (Figure 6e) and lower cell viability (Figure 6f) in ER-PTEN(G129E)-overexpressing cells. To distinguish between lipid and protein phosphatase functions at the molecular level, we investigated whether the PTEN–IP3R3 interaction was altered in ER-PTEN mutants. Both ER-PTEN(C124S) and ER-PTEN(G129E) were co-immunoprecipitate with IP3R3; however, IP3R3 preferentially interacts with the PTEN mutant that retains protein phosphatase activity. Moreover, when ER-PTEN(G129E) was present in the immunoprecipitate, the amount of co-immunoprecipitated Akt, and in particular $pAkt^{Ser473}$, were remarkably reduced. Accordingly, we detected a lower amount of pIP3R3 in ER-PTEN(G129E)-overexpressing cells (Figure 6g and Supplementary Figure 4c).

In summary, our data support a role of a fraction of ER-localized PTEN in the modulation of ER Ca^{2+} release and cellular sensitivity to Ca^{2+}-mediated apoptotic stimulation through its protein phosphatase activity. This pathway is likely to act in synergy with the plasma membrane mode of action of PTEN, thereby amplifying its capability of inducing apoptosis and tumor-suppressive effect.

Discussion

The regulation of PI3K signaling by the PIP3 lipid phosphatase activity of PTEN fulfils many of its cellular roles; however,

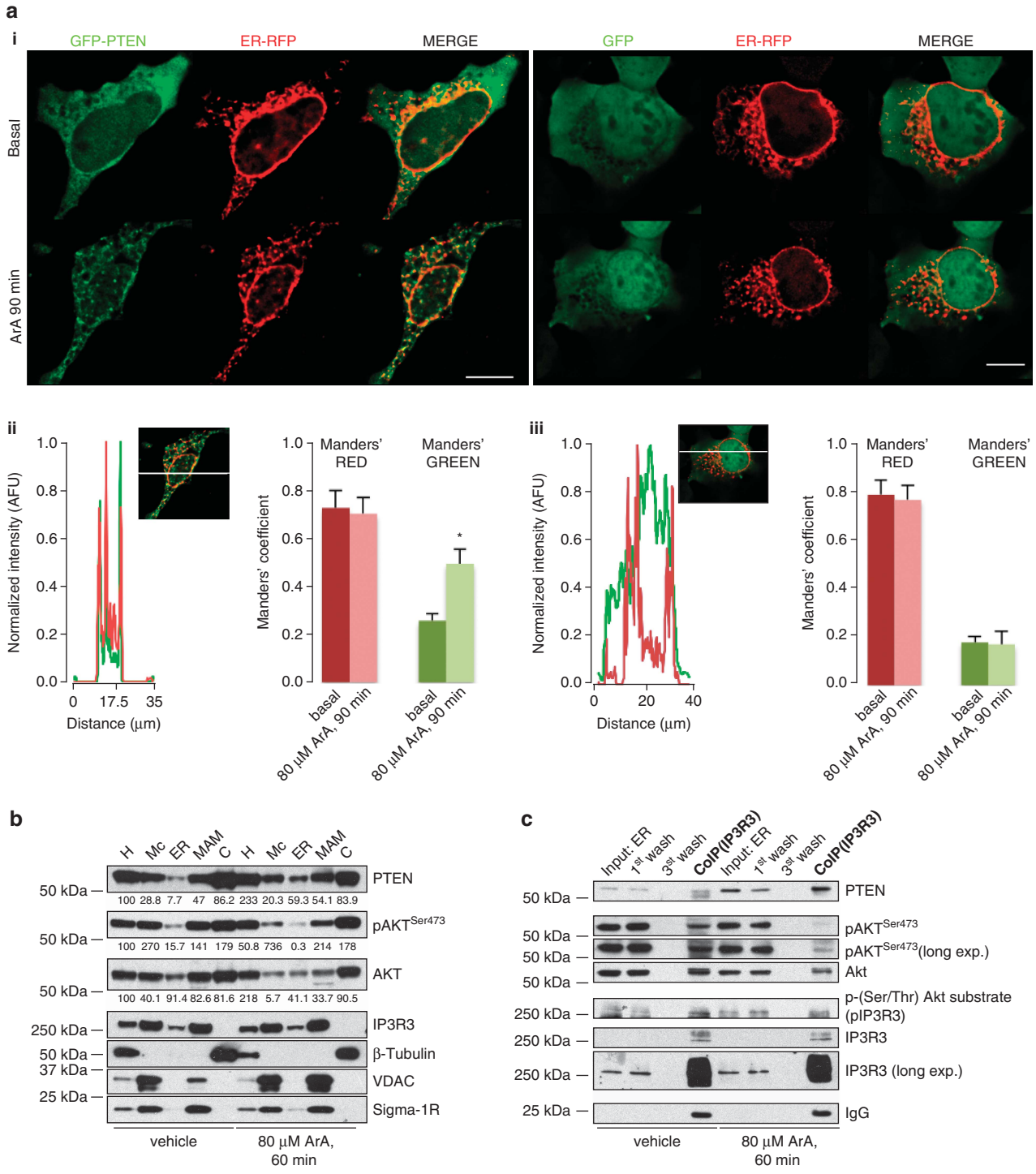

Figure 5 Ca^{2+}-dependent apoptosis induction increases PTEN localization to the ER and its interaction with IP3R3. (**d**) Colocalization between GFP-PTEN (left panels) or GFP (right panels) and ER-RFP, before and after treatment with 80 μM ArA for 90 min. The yellow signal in the merged images represents an overlapping spatial relationship between green and red fluorescence (i). The plots below show the normalized fluorescence intensity profiles after ArA treatment measured along a line of pixels that crossed the cell (thick white line in the micrograph) for GFP-PTEN and ER-RFP (ii) or GFP and ER-RFP (iii). The bar graphs show the proportion of overlap of each channel with the other for data represented in (i) using the pixel intensity spatial correlation methods of Manders. Manders' overlap coefficients are reported as mean ± S.E.M. of three independent experiments. (**b**) Immunoblot of PTEN, $pAkt^{Ser473}$ and total Akt protein levels in subcellular fractions prepared from HEK-293 cells treated with 80 μM ArA or vehicle (EtOH) for 60 min. Numbers indicate densitometrically determined protein levels relative to the marker of the corresponding fraction for Akt and PTEN or to markers normalized Akt for $pAkt^{Ser473}$. (**c**) ER fractions prepared as in (**b**) were used for co-immunoprecipitation of endogenous IP3R3 with PTEN and Akt. Using IP3R3 as bait, the levels of pIP3R3 can be detected by p-(Ser/Thr)-Akt substrates antibody reactivity at the same molecular weight of IP3R3 (~250 kDa), assuming that it represents the phosphorylation state of IP3R3.[19] In the same blot the levels of $pAkt^{Ser473}$ are shown. $^*P < 0.001$

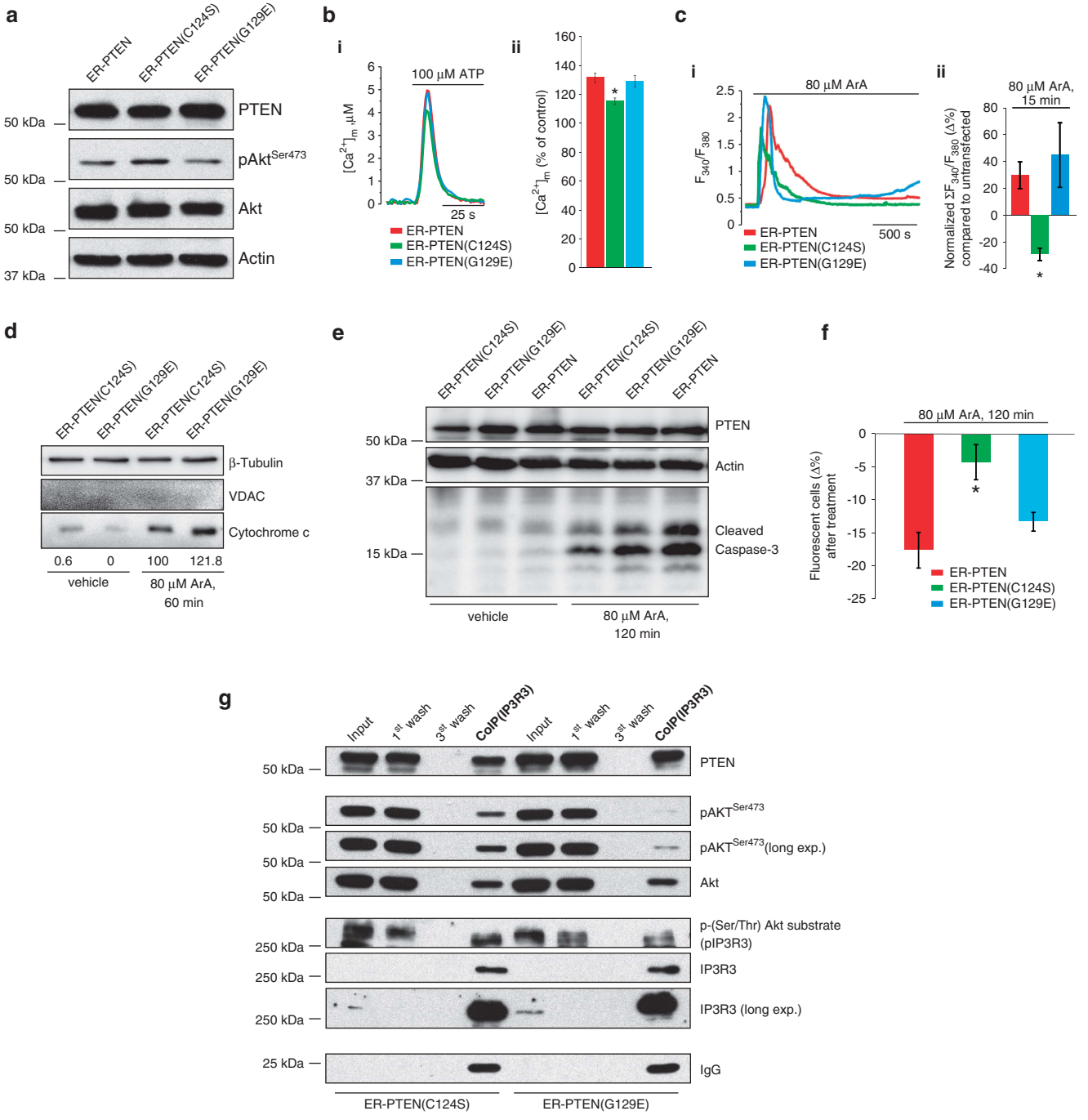

Figure 6 ER Ca^{2+} mobilization and apoptotic responses are differentially regulated by PTEN lipid and protein phosphatase activity. (**a**) PTEN expression and Akt phosphorylation were verified by WB of HEK-293 lysates transfected with ER-PTEN-, ER-PTEN(C124S)- or ER-PTEN(G129E)-encoding plasmids. (**b**) Representative traces of mitochondrial Ca^{2+} transients (i). Percentage of $[Ca^{2+}]_m$ peaks normalized to the mean of the control group (Figure 3e) (ii). (**c**) Cytosolic Ca^{2+} response induced by 80 μM ArA presented as the ratio of fluorescence at 340/380 nm (i). Change in percentage of cytosolic Ca^{2+} increases normalized as $\Sigma(F_{340}/F_{380})$ over time in comparison with untransfected cells (ii) (Δ%: 29.8 $\pm$ 10.0 for ER-PTEN; $-$29.4 $\pm$ 4.7 for ER-PTEN(C124S), $P<0.001$; 45.1 $\pm$ 24.1 for ER-PTEN(G129E). (**d**) HEK-293 cells were either transfected with plasmid encoding ER-PTEN(C124S) or ER-PTEN(G129E). Following ArA treatment, cytosolic fractions were purified and analyzed by WB for the detection of cytosolic cytochrome *c*. β-Tubulin was used as loading control and VDAC was assessed as an indicator of the purity of fractions. Representative results are reported. Numbers indicate densitometrically determined cytochrome *c* levels relative to β-tubulin. (**e**) HEK-293 cells transfected as in (**a**) were treated with 80 μM ArA or vehicle for 120 min, then total cell lysates were prepared and analyzed by WB to compare cleaved caspase-3 levels. Results are from a single experiment that is representative of three separate experiments. (**f**) Sensitivity to apoptosis in cells co-transfected with a fluorescent marker and plasmid encoding ER-PTEN, ER-PTEN(C124S) or ER-PTEN(G129E). The bars graph shows the change in percentage of fluorescent cells in the surviving cell population upon ArA treatment. *$P<0.05$. (**g**) Co-immunoprecipitation of endogenous IP3R3, Akt and ER-PTEN(C124S) or ER-PTEN(G129E). In the same blot, the levels of p-IP3R3 and pAkt^{Ser473} are shown. *$P<0.05$

emerging evidence demonstrates that other mechanisms may account for some of PTEN's functions, including protein phosphatase activity[7] and noncatalytic actions.[9] Further, despite early studies proposing that PTEN was exclusively cytoplasmic, recent reports have demonstrated that nuclear PTEN has important tumor-suppressive functions beyond its lipid phosphatase activity,[11,12,32] and some observations support the notion that PTEN can also localize to mitochondria and regulate apoptosis.[13,14] These findings highlight the possibility that different tumor-suppressive mechanisms of PTEN may occur in well-defined cellular compartments.

In this work, we investigated in greater detail the intracellular distribution of PTEN. Our results showed that a fraction of PTEN is present at the ER and MAMs. Several studies have demonstrated the importance of ER Ca^{2+} release and mitochondrial Ca^{2+} loading for triggering apoptosis.[15] Mitochondrial Ca^{2+} accumulation favors cell death and this notion is supported by numerous previous examples of pro- and anti-apoptotic proteins capable of enhancing or reducing Ca^{2+} signals, respectively.[33] For this reason, the remodeling of the Ca^{2+} signaling machinery in the ER and mitochondria of cancer cells seems imminent during oncogenic transformation, to limit death-inducing Ca^{2+} signals during cancer.[16] Growing evidence indicates that specific proteins residing at the ER and MAMs are able to regulate mitochondrial Ca^{2+} uptake.[17,34] We pursued the hypothesis that PTEN could act as a tumor suppressor, at least in part, by modulating the transmission of Ca^{2+} from the ER to mitochondria.

Our results confirmed this possibility for PTEN. In PTEN-silenced cells, a reduction in the kinetics of Ca^{2+} release from the ER that significantly blunted also the cytosolic and the mitochondrial Ca^{2+} responses, accounts for reduced sensitivity to apoptosis. However, in agreement with previous studies,[35] global PTEN overexpression did not increase the mitochondrial Ca^{2+} response after agonist stimulation. We argued that PTEN's regulation of Ca^{2+} homeostasis relied specifically on its localization to ER and MAMs. By using specific subcellular-targeted PTEN chimeras, we demonstrated that the effects of PTEN on Ca^{2+} homeostasis could not be ascribed to its regulation of PIP3 levels and subsequent Akt activation at the plasma membrane.[23,24,36,37] Indeed, the plasma membrane-targeted snap25-PTEN chimera displayed the higher reduction in Akt phosphorylation but no difference in $[Ca^{2+}]_m$. We demonstrated that ER-targeted PTEN markedly increases the $[Ca^{2+}]_m$ transients, and we found that this correlate with a more effective reduction of $pAkt^{Ser473}$ levels at the ER, in comparison with overexpression of wild-type PTEN. Unexpectedly, we observed only a slight, not statistically significant, reduction in $pAkt^{Ser473}$/Akt ratio in the MAMs fraction. As Akt is known to be present in the mitochondria in its phosphorylated active state,[38] but we were not able to detect $pAkt^{Ser473}$ in the pure mitochondria fraction, we reasoned that the inconsistency of reduced Akt phosphorylation in the MAMs fraction could arise from technical issue during the Percoll gradient centrifugation necessary to separate MAMs and pure mitochondria. Despite this, our data strongly indicate that the presence of PTEN to the ER correlate with a lower Akt activation in this organelle. PTEN localization to the ER appears to be part of the Ca^{2+}-mediated apoptotic process as further accumulation of PTEN to the ER is induced during ArA-mediated apoptosis. ArA induces Ca^{2+} release from the ER through the IP3Rs. ER-localized PTEN is able to enhance the Ca^{2+}-dependent apoptotic process by increasing the ER Ca^{2+} release in response to ER death stimuli like ArA. It is possible that early events occurring in the ER lead to tightening of the ER-mitochondrial interface (as demonstrate also by our observation of VDAC accumulation in the MAMs fraction) and are responsible for promoting some apoptotic mechanisms.[26,28,29] This explains the apparent ineffectiveness of wild-type PTEN in comparison with ER-PTEN; the latter, being already at the ER surface, is straightaway ready for acting on its molecular target. PTEN loss or mutations resulting in its inability to be targeted to the ER and MAMs could limit apoptosis-inducing Ca^{2+} signals during cancer.

Co-immunoprecipitation experiments showed that PTEN interacts with IP3R3, together with Akt, providing a molecular route for its modulation of Ca^{2+} signaling. Akt can phosphorylate all IP3R isoforms,[36,37] and a specific activity of Akt on IP3R3 leads to diminished ER-to-mitochondria Ca^{2+} transfer and protection from apoptosis.[19,24] The functional importance of PTEN interaction with IP3R3 is highlighted by the demonstration that, during apoptotic stimulation, the enhanced ER localization of PTEN positively correlated with an increased interaction with IP3R3, whereas Akt amount and phosphorylation levels as well as IP3R3 phosphorylation were reduced. The modulation of Akt-dependent phosphorylation of IP3Rs exerted by ER-localized PTEN could reveal a further level of PTEN-mediated inhibition of Akt activity, beyond its plasma membrane lipid phosphatase activity. We concluded that PTEN's regulation of Ca^{2+} homeostasis relied specifically on its ability to counteract Akt-mediated IP3R3 phosphorylation, directly from the ER side. This also explain why—despite the OMM being a fundamental part of the MAMs—we observed no difference in $[Ca^{2+}]_m$ with AKAP-PTEN.

To address the relative importance of the lipid and protein phosphatase activity of PTEN in the regulation of ER-mitochondria interorganelle Ca^{2+} signaling, we have targeted two functional mutants, PTEN C124S (phosphatase dead) and PTEN G129E (retained protein phosphatase only), to the outer ER surface. When we overexpressed ER-PTEN (C124S), Ca^{2+} signaling after agonist- or apoptotic-induced Ca^{2+} release, and cell sensitivity to the apoptotic stimulus, was comparable with those in control cells. Conversely, cells overexpressing ER-PTEN(G129E) retained the same Ca^{2+} responses and sensitivity to Ca^{2+}-dependent cell death as ER-PTEN. In comparison with ER-PTEN(C124S), ER-PTEN(G129E) displayed a more effective interaction with IP3R3 but reduced Akt and drastically lowered $pAkt^{Ser473}$ levels in the co-immunoprecipitate, in addition to decreased IP3R3 phosphorylation that explains the enhanced ER Ca^{2+} release. However, at present, the precise molecular substrate of PTEN's protein phosphatase activity remains to be identified.

Overall, these results reveal that a subpopulation of PTEN is localized at the ER-MAMs interface with mitochondria, where it regulates ER-to-mitochondria Ca^{2+} signaling and exerts a pro-apoptotic activity. We provide evidence for a novel mechanism by which the ER pool of PTEN can

counteract Akt activation and thus can inhibit the Akt-mediated phosphorylation of IP3R3 that protects from Ca^{2+}-mediated apoptosis. Our findings allow us to conclude that the novel function of ER-localized PTEN presented herein specifically relies on its protein phosphatase activity.

Materials and Methods

Cells culture and transfection. HEK-293 cells were grown in Dulbecco's modified Eagle's medium (DMEM) (Euroclone, Milan, Italy), supplemented with 10% fetal bovine serum (FBS). MEFs were collected from E13.5 embryos and maintained in culture in DMEM supplemented with 10% FBS. HEK-293 cells were seeded 48 h before transfection onto round glass coverslips coated with poly-L-lysine (Sigma, St. Louis, MO, USA), 13 mm in diameter for aequorin experiments or 24 mm for Fura-2/AM measurements and IF. For immunoblot and cell death experiments, cells were seeded on 10-cm petri dishes. Cells were allowed to grow to 50% confluence, then transfected with a standard calcium phosphate procedure and used in the experiments 36-h post-transfection.

Treatments with 80-μM ArA were carried out in Krebs-Ringer buffer (KRB: 135 mM NaCl, 5 mM KCl, 1 mM $MgSO_4$, 0.4 mM KH_2PO_4, 5.5 mM glucose, 20 mM HEPES, pH 7.4) supplemented with 1 mM $CaCl_2$.

Plasmid cloning. To silence PTEN, specific siRNA was designed by using Oligoengine RNAi design tool: siPTEN(1049), nucleotides 1049–1067 of the corresponding mRNA (5′-AGTAGAGGAGCCGTCAAAT-3′); siPTEN(219), nucleotides 219–237 of the corresponding mRNA (5′-AGACATTATGACACCGCCA-3′). Oligonucleotides containing the selected sequences were purchased from Sigma-Aldrich and cloned into pSUPER (Oligoengine, Seattle, WA, USA) according to the manufacturer's instructions.

Human PTEN, GFP-PTEN, GFP-PTEN[NLS] and GFP-PTEN[NES] have been described previously.[21] For constructing ER-PTEN, a sequence from UBC6[19] was subcloned (KpnI/BamHI) to the N-terminus of human PTEN cloned (EcoRI/EcoRI) into pcDNA3.1. AKAP-PTEN was constructed by fusing the mouse AKAP1 sequence (from OMM-IP3R-LBD,[4] amplified as BglII-HindIII and then subcloned HindIII/HindIII) to the N-terminus of human PTEN. For generating snap25-PTEN, the SNAP-25 coding sequence was amplified from SNAP-25-aequorin[39] and then subcloned (KpnI/BamHI) to the N-terminus of human PTEN. ER-PTEN(C124S) and ER-PTEN(G129E) were obtained by substituting the human PTEN coding sequence of ER-PTEN with those of human PTEN(C124S) or (G129E) mutants[12] (subcloned EcoRI/XhoI).

Subcellular fractionation. Cell fractionation was performed using HEK-293 and MEFs cells as previously described.[18] Cells (10^9) were harvested, washed by centrifugation at 500 *g* for 5 min with PBS (supplemented with 2 mM Na_3VO_4 and 2 mM NaF when preservation of protein phosphorylation states was required), resuspended in homogenization buffer (225 mM mannitol, 75 mM sucrose, 30 mM Tris-HCl pH 7.4, 0.1 mM EGTA and PMSF) and gently disrupted by Dounce homogenization. The homogenate was centrifuged twice at 600 *g* for 5 min to remove nuclei and unbroken cells, and then the supernatant was centrifuged at 10 300 $\times$ *g* for 10 min to pellet crude mitochondria. The resultant supernatant was centrifuged at 20 000 $\times$ *g* for 30 min at 4 °C. The pellet consists of lisosomal and plasma membrane fractions. Further centrifugation of the obtained supernatant at 100 000 $\times$ *g* for 90 min (70-Ti rotor; Beckman, Milan, Italy) at 4 °C results in the isolation of ER (pellet) and cytosolic fraction (supernatant). The crude mitochondrial fraction, resuspended in isolation buffer (250 mM mannitol, 5 mM HEPES pH 7.4 and 0.5 mM EGTA), was subjected to Percoll gradient centrifugation (Percoll medium: 225 mM mannitol, 25 mM HEPES pH 7.4, 1 mM EGTA and 30% vol/vol Percoll) in a 10-ml polycarbonate ultracentrifuge tube. After centrifugation at 95 000 *g* for 30 min (SW40 rotor), a dense band containing purified mitochondria was recovered approximately 3/4 down the tube, washed by centrifugation at 6300 $\times$ *g* for 10 min to remove the Percoll and finally resuspended in isolation medium. The MAMs, containing the structural contacts between mitochondria and ER, were removed from the Percoll gradient as a diffuse white band located above the mitochondria, were diluted in isolation buffer and centrifuged at 6300 $\times$ *g* for 10 min; then the supernatant was further centrifuged at 100 000 $\times$ *g* for 90 min (70-Ti rotor, Beckman) to pellet the MAMs fraction. When preservation of protein phosphorylation states was required, immediately after the recovery, 2 mM Na_3VO_4 and 2 mM NaF were added to each fractions.

For PK assay the crude mitochondrial fraction was isolated in mitochondrial buffer (10 mM Tris/MOPS, pH 7.4, 0.1 mM EGTA, 250 mM sucrose) and subjected to 100 μM PK (Sigma) for 30 min on ice.

Co-immunoprecipitation. Co-immunoprecipitations were carried out using protein G-coated sepharose beads (GE Healthcare, Chalfont St. Giles, UK) following the manufacturer's instructions. For whole-cell extracts, cells were lysed in buffer containing 30 mM Tris-HCl (pH 7.4), 50 mM NaCl, 1% NP-40 and cleared by centrifugation. Protein extractions in the ER fraction were carried out by adding 50 mM NaCl and 1% NP-40 to the homogenization buffer. All the buffers were supplemented with proteases and phosphatases inhibitors (2 mM Na_3VO_4, 2 mM NaF, 1 mM PMSF and protease inhibitor cocktail). Extracted proteins (1000 μg) were first precleared by incubating lysates with sepharose beads for 1 h at 4 °C and the supernatant (referred as Input) was incubated overnight with IP3R3 antibody at 4 °C. Precipitation of the immune complexes was carried for 4 h at 4 °C. Afterwards, beads were washed with 50 mM Tris-HCl pH 7.4, 0.1% NP-40 4 °C supplemented with phosphatases inhibitors and PMSF. Samples were proceed by SDS-PAGE and analyzed by standard western blotting technique.

Western blot. Total cell lysates were prepared in RIPA buffer (50 mM Tris-HCl pH 7.8, 150 mM NaCl, 1% IGEPAL CA-630, 0.5% sodium deoxycholate, 0.1% SDS, 1 mM DTT) supplemented with proteases and phosphatases inhibitors (2 mM Na_3VO_4, 2 mM NaF, 1 mM PMSF and protease inhibitor cocktail). Alternatively, cytosolic extracts were obtained by digitonin permeabilization, as previously described.[40] Proteins were quantified using the Bradford assay (Bio-Rad Laboratories, Hercules, CA, USA), separated by SDS-PAGE and transferred to nitrocellulose membranes for standard western blotting. Antibodies were purchased from the following sources and used at the indicated dilutions: PTEN (1 : 1000), Akt (1 : 1000), $pAkt^{Ser473}$ (1 : 500), p-(Ser/Thr) Akt substrate (1 : 500) and Caspase-3 (1 : 500) from Cell Signaling (Danvers, MA, USA); actin (1 : 3000), Sigma-1R (1 : 1000) and β-tubulin (1 : 3000) from Sigma-Aldrich; Cytochrome c (1 : 10000) IP3R3 (1 : 300) from BD Biosciences (San Jose, CA, USA); FACL4 (1 : 250), HK-I (1 : 1000) and SOD-2 (1 : 1000) from Santa Cruz (Santa Cruz, CA, USA); and lamin B1 (1 : 1000) and VDAC (1 : 3000) from Abcam (Cambridge, UK). Membranes were incubated with appropriate horseradish peroxidase-conjugated secondary antibodies (Santa Cruz), followed by chemiluminescence detection (Thermo Scientific-Pierce, Waltham, MA, USA).

Immunofluorescence. HEK-293 cells were stained with 0.25 μg/ml Hoechst for 10 min at 37 °C and then fixed in 4% paraformaldehyde in PBS for 15 min. After three washes with PBS, the cells were permeabilized for 10 min with 0.1% Triton X-100 in PBS and then blocked in PBS containing 1% BSA for 20 min. Cells were incubated O/N at 4 °C with the PTEN (A2B1) antibody (1 : 50, Santa Cruz) and for double staining with the PDI antibody (1 : 100, Abcam). Finally, primary antibodies were revealed by means of appropriate AlexaFluor 488 conjugates for PTEN or AlexaFluor 633 conjugates for PDI (Life Technologies, Carlsbad, CA, USA). After each antibody incubation, the cells were washed three times with 0.1% Triton X-100 in PBS. Images were acquired on an Axiovert 220 M microscope equipped with a $\times$ 100 oil immersion Plan-Neofluar objective (NA 1.3, from Carl Zeiss, Jena, Germany) and a CoolSnap HQ CCD camera. Each field was acquired over 26 z-planes spaced by 0.4 μm. Image sampling was below resolution limit and calculated according to the Nyquist calculator (available at http://www.svi.nl/NyquistCalculator). After acquisition, z-stacks were deconvoluted with the 'Parallel Iterative Deconvolution' plugin of the open source Fiji software (freely available at http://fiji.sc/).

Aequorin measurements. All aequorin measurements were performed as previously described.[20] HEK-293 cells grown on 13-mm round glass coverslips were co-transfected with 1 μg of aequorin (endoplasmic reticulum-targeted mutated aequorin, erAEQmut, cytosolic aequorin, cytAEQ or mitochondria-targeted aequorin, mtAEQ) and 3 μg of the indicated siRNA or plasmid. After 36 h, the cells were reconstituted and placed in a perfused thermostated chamber where the light signal was collected in a purpose-built luminometer and calibrated into $[Ca^{2+}]$ values. Cells transfected with erAEQmut were reconstituted with coelenterazine n (Tebu-Bio, Le-Perray-en-Yvelines, France), after ER Ca^{2+} depletion by incubating cells for 1 h at 4 °C in KRB supplemented with 100 μM EGTA and 40 μM tBHQ (2,5-Di-*tert*-butylhydroquinone) (Sigma); cells were then washed with KRB supplemented with 2% BSA and 1 mM EGTA. Cells transfected with cytAEQ and mtAEQ were reconstituted with coelenterazine (Synchem,

Felsberg/Altenburg, Germany) for 2 h in KRB supplemented with 1 mM $CaCl_2$. All aequorin measurements were carried out in 1 mM Ca^{2+}/KRB (cytAEQ and mtAEQ) or 100 μM EGTA/KRB (erAEQmut). ER refilling was trigger by perfusing with 1 mM Ca^{2+}/KRB until steady state was reached. Agonist was added to the same medium, as specified in the figures. The experiments were finish by lysing the cells with 100 μM digitonin in a hypotonic Ca^{2+}-rich solution (10 mM $CaCl_2$ in H_2O).

Fura-2/AM measurements. Cytosolic Ca^{2+} response was evaluated using the fluorescent Ca^{2+} indicator Fura-2/AM (Life Technologies), as previously described.[23] HEK-293 cells were grown on 24-mm coverslips and co-transfected with 4 μg on the indicated siRNA or plasmid and 4 μg of mtDsRED in order to identify transfected cells in single-cell imaging experiments. Untransfected cells in the same sample were used to compare changes in the 340/380 Fura-2/AM ratio. After 36 h, cells were incubated at 37 °C for 30 min in 1 mM Ca^{2+}/KRB supplemented with 2.5 μM Fura-2/AM, 0.02% Pluronic F-68 (Sigma), 0.1 mM Sulfinpyrazone (Sigma). Cells were then washed and supplied with 1 mM Ca^{2+}/KRB. To determine cytosolic Ca^{2+} response, the cells were placed in an open Leyden chamber on a 37 °C thermostatted stage and exposed to 340/380 wavelength light using the Olympus xcellence multiple wavelength high-resolution fluorescence microscopy system. The fluorescence data collected were expressed as emission ratios. To pharmacologically inhibit Ca^{2+} release via IP3Rs, the cells were preincubated in culture medium supplemented with 2 μM XeC for 16 h, and then Fura-2/AM loading and Ca^{2+} release recording upon stimulation with 80 μM ArA were performed in 1 mM Ca^{2+}/KRB supplemented with 2 μM XeC. For experiments in Ca^{2+}-free conditions, after Fura-2/AM loading cells were washed in KRB, and 1 mM EGTA was added after 15 s of fluorescence data collection before stimulation with 80 μM ArA.

Quantitative colocalization analysis. HEK-293 cells were seeded on 24-mm coverslips previously coated with poly-L-lysine. At 36 h after plating, cells were either transfected with GFP or GFP-tagged PTEN (GFP-PTEN) using calcium phosphate method. At 24 h after transfection, cells were transduced with CellLight ER-RFP BacMam 2.0 (Life Technologies), according to the manufacturer's protocol. Then, time-lapse recording of GFP-PTEN dynamics during 80-μM ArA treatment for 90 min was performed with a Nikon Swept Field Confocal equipped with CFI Plan Apo VC60XH objective (numerical aperture, 1.4) (Nikon Instruments, Melville, NY, USA) and an Andor DU885 electron multiplying charge-coupled device (EM-CCD) camera (Andor Technology Ltd, Belfast, Northern Ireland), the overall image sampling was below the resolution limit (X and Y pixel size: 133 nm). Coverslips were placed in an incubated chamber with controlled temperature, CO_2 and humidity; images were then acquired with a differential frequency during the experiment: cells were placed in 1 mM Ca^{2+} KRB and basal fluorescence images were acquired for 5 min; then cells were stimulated with ArA (80 μM final), and fluorescence images were acquired for 1 h and 30 min (in order to avoid bleaching of the fluorophores, images were acquired each 3 min for 30 min, and then each 10 min for the remaining time). Acquired images were then analyzed by using open source software Fiji. Images were corrected for spectral bleedthrough using the Spectral Unmixing plugin (available at http://rsbweb.nih.gov/ij/plugins/spectral-unmixing.html). Then, single cells were analyzed, and, for each of those, the Manders' overlap coefficient were obtained using the JACOP plugin.[41] Cells with a significant increase at the end of the experiment compared with the beginning were considered translocated (for $P<0.001$).

Cell death. For assessed cell sensitivity to apoptosis, HEK-293 cells were co-transfected with H2B-RFP fluorescent marker and the indicated siRNA, plasmid or empty vector in a 1 : 1 ratio. The effect on cell fate was evaluated by applying the apoptotic challenge ArA and comparing the survival of transfected and non-transfected cells. For induction of apoptosis, growth media was replaced with 1 mM Ca^{2+}/KRB containing 80 μM ArA (Santa Cruz). After ArA treatment, the cells were extensively washed with 1 mM Ca^{2+}/KRB and the relative amount of H2B-RFP-positive cells in the surviving population was calculated using the Tali Image-Based Cytometer (Life Technologies) (mean transfection efficiency were roughly 60% for all conditions). As described in previous paper for other genes of interest,[28] in mock-transfected cells, although the total number of cells is reduced after cell death induction, the apparent transfection efficiency was maintained (i.e., transfected and non- transfected cells have the same sensitivity to the apoptotic stimulus and thus die to the same extent). However, when cells are transfected with a construct influencing their sensitivity to apoptosis, this will be reflected by a change in the fraction of fluorescent cells, that is, in the 'apparent' transfection efficiency. Thus, protection from apoptosis results into an apparent increase of transfection, whereas a decrease reflects a higher sensitivity to apoptosis. Data are reported as the mean percentage change in the apparent transfection efficiency after apoptotic challenge compared with vehicle-treated cells.

Statistical analyses. Statistical analyses were performed using Student's *t*-test. A *P*-value ≤ 0.05 was considered significant. All data are reported as mean $\pm$ S.E.M..

Conflict of Interest

The authors declare no conflict of interest.

Acknowledgements. We thank G Merli for carrying out some experiments and members of the Pinton lab for stimulating discussions. This research was supported by AIRC, Telethon (GGP09128), the Italian Ministry of Education, University and Research (COFIN and FIRB), the Italian Cystic Fibrosis Research Foundation and the Italian Ministry of Health to PP. AB was supported by a research fellowship (FISM: Cod. 2010/B/1); SM was supported by a FIRC fellowship.

1. Salmena L, Carracedo A, Pandolfi PP. Tenets of PTEN tumor suppression. *Cell* 2008; **133**: 403–414.
2. Eng C. PTEN: one gene, many syndromes. *Hum Mutat* 2003; **22**: 183–198.
3. Maehama T, Dixon JE. The tumor suppressor, PTEN/MMAC1, dephosphorylates the lipid second messenger, phosphatidylinositol 3,4,5-trisphosphate. *J Biol Chem* 1998; **273**: 13375–13378.
4. Myers MP, Stolarov JP, Eng C, Li J, Wang SI, Wigler MH *et al.* P-TEN, the tumor suppressor from human chromosome 10q23, is a dual-specificity phosphatase. *Proc Natl Acad Sci USA.* 1997; **94**: 9052–9057.
5. Stambolic V, Suzuki A, de la Pompa JL, Brothers GM, Mirtsos C, Sasaki T *et al.* Negative regulation of PKB/Akt-dependent cell survival by the tumor suppressor PTEN. *Cell* 1998; **95**: 29–39.
6. Chalhoub N, Baker SJ. PTEN and the PI3-kinase pathway in cancer. *Annu Rev Pathol* 2009; **4**: 127–150.
7. Tamura M, Gu J, Matsumoto K, Aota S, Parsons R, Yamada KM. Inhibition of cell migration, spreading, and focal adhesions by tumor suppressor PTEN. *Science* 1998; **280**: 1614–1617.
8. Raftopoulou M, Etienne-Manneville S, Self A, Nicholls S, Hall A. Regulation of cell migration by the C2 domain of the tumor suppressor PTEN. *Science* 2004; **303**: 1179–1181.
9. Okumura K, Zhao M, Depinho RA, Furnari FB, Cavenee WK. Cellular transformation by the MSP58 oncogene is inhibited by its physical interaction with the PTEN tumor suppressor. *Proc Natl Acad Sci USA.* 2005; **102**: 2703–2706.
10. Funamoto S, Meili R, Lee S, Parry L, Firtel RA. Spatial and temporal regulation of 3-phosphoinositides by PI 3-kinase and PTEN mediates chemotaxis. *Cell* 2002; **109**: 611–623.
11. Shen WH, Balajee AS, Wang J, Wu H, Eng C, Pandolfi PP *et al.* Essential role for nuclear PTEN in maintaining chromosomal integrity. *Cell* 2007; **128**: 157–170.
12. Song MS, Carracedo A, Salmena L, Song SJ, Egia A, Malumbres M *et al.* Nuclear PTEN regulates the APC-CDH1 tumor-suppressive complex in a phosphatase-independent manner. *Cell* 2011; **144**: 187–199.
13. Zhu Y, Hoell P, Ahlemeyer B, Krieglstein J. PTEN: a crucial mediator of mitochondria-dependent apoptosis. *Apoptosis* 2006; **11**: 197–207.
14. Zu L, Zheng X, Wang B, Parajuli N, Steenbergen C, Becker LC *et al.* Ischemic preconditioning attenuates mitochondrial localization of PTEN induced by ischemia-reperfusion. *Am J Physiol Heart Circ Physiol* 2011; **300**: H2177–H2186.
15. Pinton P, Giorgi C, Siviero R, Zecchini E, Rizzuto R. Calcium and apoptosis: ER-mitochondria Ca2+ transfer in the control of apoptosis. *Oncogene* 2008; **27**: 6407–6418.
16. Roderick HL, Cook SJ. Ca2+ signalling checkpoints in cancer: remodelling Ca2+ for cancer cell proliferation and survival. *Nat Rev Cancer* 2008; **8**: 361–375.
17. Bononi A, Missiroli S, Poletti F, Suski JM, Agnoletto C, Bonora M *et al.* Mitochondria-Associated Membranes (MAMs) as Hotspot Ca(2+) Signaling Units. *Adv Exp Med Biol* 2012; **740**: 411–437.
18. Wieckowski MR, Giorgi C, Lebiedzinska M, Duszynski J, Pinton P. Isolation of mitochondria-associated membranes and mitochondria from animal tissues and cells. *Nat Protoc* 2009; **4**: 1582–1590.
19. Giorgi C, Ito K, Lin HK, Santangelo C, Wieckowski MR, Lebiedzinska M *et al.* PML regulates apoptosis at endoplasmic reticulum by modulating calcium release. *Science* 2010; **330**: 1247–1251.

20. Pinton P, Rimessi A, Romagnoli A, Prandini A, Rizzuto R. Biosensors for the detection of calcium and pH. *Methods Cell Biol* 2007; **80**: 297–325.
21. Trotman LC, Wang X, Alimonti A, Chen Z, Teruya-Feldstein J, Yang H *et al.* Ubiquitination regulates PTEN nuclear import and tumor suppression. *Cell* 2007; **128**: 141–156.
22. Scorrano L, Oakes SA, Opferman JT, Cheng EH, Sorcinelli MD, Pozzan T *et al.* BAX and BAK regulation of endoplasmic reticulum Ca2+: a control point for apoptosis. *Science* 2003; **300**: 135–139.
23. Marchi S, Rimessi A, Giorgi C, Baldini C, Ferroni L, Rizzuto R *et al.* Akt kinase reducing endoplasmic reticulum Ca2+ release protects cells from Ca2+-dependent apoptotic stimuli. *Biochem Biophys Res Commun* 2008; **375**: 501–505.
24. Marchi S, Marinello M, Bononi A, Bonora M, Giorgi C, Rimessi A *et al.* Selective modulation of subtype III IP(3)R by Akt regulates ER Ca(2)(+) release and apoptosis. *Cell Death Dis* 2012; **3**: e304.
25. Gafni J, Munsch JA, Lam TH, Catlin MC, Costa LG, Molinski TF *et al.* Xestospongins: potent membrane permeable blockers of the inositol 1,4,5-trisphosphate receptor. *Neuron* 1997; **19**: 723–733.
26. Csordas G, Renken C, Varnai P, Walter L, Weaver D, Buttle KF *et al.* Structural and functional features and significance of the physical linkage between ER and mitochondria. *J Cell Biol* 2006; **174**: 915–921.
27. Szabadkai G, Bianchi K, Varnai P, De Stefani D, Wieckowski MR, Cavagna D *et al.* Chaperone-mediated coupling of endoplasmic reticulum and mitochondrial Ca2+ channels. *J Cell Biol* 2006; **175**: 901–911.
28. De Stefani D, Bononi A, Romagnoli A, Messina A, De Pinto V, Pinton P *et al.* VDAC1 selectively transfers apoptotic Ca(2+) signals to mitochondria. *Cell Death Differ* 2012; **19**: 267–273.
29. Bravo R, Vicencio JM, Parra V, Troncoso R, Munoz JP, Bui M *et al.* Increased ER-mitochondrial coupling promotes mitochondrial respiration and bioenergetics during early phases of ER stress. *J Cell Sci* 2011; **124**(Pt 13): 2143–2152.
30. Mendes CC, Gomes DA, Thompson M, Souto NC, Goes TS, Goes AM *et al.* The type III inositol 1,4,5-trisphosphate receptor preferentially transmits apoptotic Ca2+ signals into mitochondria. *J Biol Chem* 2005; **280**: 40892–40900.
31. Myers MP, Pass I, Batty IH, Van der Kaay J, Stolarov JP, Hemmings BA *et al.* The lipid phosphatase activity of PTEN is critical for its tumor supressor function. *Proc Natl Acad Sci USA.* 1998; **95**: 13513–13518.
32. Chung JH, Eng C. Nuclear-cytoplasmic partitioning of phosphatase and tensin homologue deleted on chromosome 10 (PTEN) differentially regulates the cell cycle and apoptosis. *Cancer Res* 2005; **65**: 8096–8100.
33. Giorgi C, Baldassari F, Bononi A, Bonora M, De Marchi E, Marchi S *et al.* Mitochondrial Ca(2+) and apoptosis. *Cell Calcium* 2012; **52**: 36–43.
34. Grimm S. The ER-mitochondria interface: the social network of cell death. *Biochim Biophys Acta* 2012; **1823**: 327–334.
35. Garcia-Cao I, Song MS, Hobbs RM, Laurent G, Giorgi C, de Boer VC *et al.* Systemic elevation of PTEN induces a tumor-suppressive metabolic state. *Cell* 2012; **149**: 49–62.
36. Szado T, Vanderheyden V, Parys JB, De Smedt H, Rietdorf K, Kotelevets L *et al.* Phosphorylation of inositol 1,4,5-trisphosphate receptors by protein kinase B/Akt inhibits Ca2+ release and apoptosis. *Proc Natl Acad Sci USA.* 2008; **105**: 2427–2432.
37. Khan MT, Wagner L 2nd, Yule DI, Bhanumathy C, Joseph SK. Akt kinase phosphorylation of inositol 1,4,5-trisphosphate receptors. *J Biol Chem* 2006; **281**: 3731–3737.
38. Bijur GN, Jope RS. Rapid accumulation of Akt in mitochondria following phosphatidylinositol 3-kinase activation. *J Neurochem* 2003; **87**: 1427–1435.
39. Marsault R, Murgia M, Pozzan T, Rizzuto R. Domains of high Ca2+ beneath the plasma membrane of living A7r5 cells. *EMBO J.* 1997; **16**: 1575–1581.
40. Arnoult D. Apoptosis-associated mitochondrial outer membrane permeabilization assays. *Methods* 2008; **44**: 229–234.
41. Bolte S, Cordelieres FP. A guided tour into subcellular colocalization analysis in light microscopy. *J Microsc* 2006; **224**(Pt 3): 213–232.

Supplementary Information accompanies this paper on Cell Death and Differentiation website (http://www.nature.com/cdd)

Supplementary information

Identification of PTEN at the ER and MAMs and its regulation of Ca^{2+} signaling and apoptosis in a protein phosphatase-dependent manner

Angela Bononi, Massimo Bonora, Saverio Marchi, Sonia Missiroli, Federica Poletti, Carlotta Giorgi, Pier Paolo Pandolfi and Paolo Pinton

Supplementary Figure Legends

Supplementary Figure 1. Intracellular distributions of PTEN in MEFs. Protein components of subcellular fractions prepared from mouse embryonic fibroblast (MEF) cells were loaded on 10% SDS-polyacrylamide gels and revealed by western blot. PTEN was detected with a specific monoclonal antibody. Marker proteins indicate ER (IP3R3), MAMs (FACL4), cytosol (β-tubulin), nucleus (PCNA) and mitochondria (SOD-2). H: homogenate; Mc: crude mitochondrial fraction; Mp: pure mitochondrial fraction; ER; MAMs; C: cytosol.

Supplementary Figure 2. Densitometric analysis and plotting of Akt phosphorylation status presented as the ratio between phosphorylated and total protein. Quantification of WB analysis on HEK-293 lysates from mock- (control) or siRNAs-PTEN transfected cells (**a**), and form cells transfected with either control, PTEN, GFP-PTEN[NLS], GFP-PTEN[NES], snap25-PTEN, AKAP-PTEN or ER-PTEN encoding plasmids (**b**). Densitometry of band intensity is expressed relative to control (100%). Data are mean ± SEM from 3 to 5 independent experiments. (**c**) Quantification of Akt phosphorylation in subcellular fractions prepared from HEK-293 cells transfected with recombinant wild type PTEN or ER-PTEN encoding plasmids. Densitometric

analysis of $pAkt^{Ser473}$/Akt bands intensity in homogenate (H), crude mitochondria (Mc), ER, MAM and cytosol (C), is expressed relative to PTEN overexpressing cells (100%). Data are mean ± SEM for 3 independent experiments. * indicates $P < 0.05$.

Supplementary Figure 3. Effects of ArA on intracellular Ca^{2+} mobilization, apoptotic responses and PTEN interaction with IP3R3, Related to Figures 4 and 5. (**a**) Fura-2/AM measurements in HEK-293 cells preincubated with 2 μM xestospongin C (XeC) or vehicle for 16 hours. XeC is a membrane-permeable inhibitor of the IP3-mediated Ca^{2+} release when used at low micromolar concentrations. In the presence of XeC, the increase of $[Ca^{2+}]_c$ in response to 80 μM ArA was significantly depressed, suggesting that the latter involved Ca^{2+} release via IP3R. (**i**) Typical tracing of the $[Ca^{2+}]_c$ response is presented as a 340/380 nm ratio. Each of the traces shown is representative of at least three independent experiments. (**ii**) Bars graphs (mean ± SEM) show the change in percentage of cytosolic Ca^{2+} increases normalized as $\Sigma(F_{340}/F_{380})$ over time, in comparison to cells incubated with vehicle. (**b**) Fura-2/AM measurements in Ca^{2+}-free medium. HEK-293 cells overexpressing PTEN, ER-PTEN, or mock-transfected, were loaded with Fura-2/AM. Where indicated, Ca^{2+}-free conditions were obtained as described in Materials and Methods. The basal fluorescence signal was monitored prior to treatment: 1 mM EGTA was added to Ca^{2+}-free medium at 15 s to chelate residual Ca^{2+}, and 80 μM ArA was added at 75 s. Under these conditions, the addition of ArA still stimulated an initial increase in intracellular free Ca^{2+}, however, the slower subsequent rise in intracellular Ca^{2+} which was detected in the presence of extracellular Ca^{2+} (Figures 4a-i and 4b-i) was not observed. (**i**) The kinetic behavior of the $[Ca^{2+}]_c$ response is presented as a 340/380 nm ratio. Each of the traces shown is representative of at least three independent experiments. (**ii**) Bars graphs (mean ± SEM) show the change in percentage of cytosolic Ca^{2+} increases normalized as $\Sigma(F_{340}/F_{380})$ over time, in comparison to untransfected cells. (**c**) Densitometric analysis of normalized cleaved caspase-3 protein levels in HEK-293 cells treated with 80 μM ArA for 120 min. In the bar graphs mean ± SEM is expressed relative to control mock-tranfected cells (100%), for 4 independent experiments. (**d**) Quantification of CoIP data presented in Figure 5c. Protein levels were normalized to the IgG light chain bands. Densitometry of bands intensity is expressed relative to untreated control (100%). Data are mean ± SEM for 3 independent experiments.

Supplementary Figure 4. Regulation of ER Ca^{2+} mobilization requires PTEN protein, but not lipid, phosphatase activity, Related to Figure 6. (**a**) Densitometric quantification of WB and plotting of the $pAkt^{Ser473}$/Akt ratios is expressed relative to ER-PTEN transfected cells (100%).

Normalization between phosphorylated Akt and Akt indicates an increased of phosphorylation in HEK-293 cells lysate from ER-PTEN(C124S) transfected HEK-293 cells in comparison to ER-PTEN or ER-PTEN(G129E) transfected cells. Data are mean ± SEM for 5 independent experiments. (**b**) HEK-293 cells overexpressing ER-PTEN, ER-PTEN(C124S), ER-PTEN(G129E) or mock-transfected, were loaded with Fura-2/AM to measure changes in intracellular Ca^{2+} response induced by ArA in Ca^{2+}-free conditions, as in Supplementary Figure 3a. (**i**) The kinetic behavior of the $[Ca^{2+}]_c$ response is presented as a 340/380 nm ratio. Each of the traces shown is representative of at least three independent experiments. (**ii**) Bars graphs (mean ± SEM) show the change in percentage of cytosolic Ca^{2+} increases normalized as $\Sigma(F_{340}/F_{380})$ over time, in comparison to untransfected cells. (**c**) Quantification of CoIP data presented in Figure 6g. Protein levels were normalized to the IgG light chain bands. Densitometry of bands intensity is expressed relative to ER-PTEN(C124S) transfected cells (100%). Data are mean ± SEM for 3 independent experiments. * indicates $P < 0.05$.

Supplementary Video data. Increased localization of PTEN at the ER induced by ArA treatment, Related to Figure 5. Cells were transfected with GFP tagged PTEN (GFP-PTEN) or GFP. At 48 hours after transfection, cells were labeled with ER-tracker RED (Life Technologies), according to the manufacturer's protocol. Time-lapse recording during 80 μM ArA treatment was performed as in Figure 5a. (**Video 1** and **Video 2**) Time-lapse recording of GFP-PTEN dynamics during ArA treatment; GFP-PTEN (left), ER-Tracker (middle) and merged (right). (**Video 3**) Time-lapse recording of GFP dynamics during ArA treatment; GFP (left), ER-Tracker (middle) and merged (right). Times are shown in the bottom left corner of the frame.

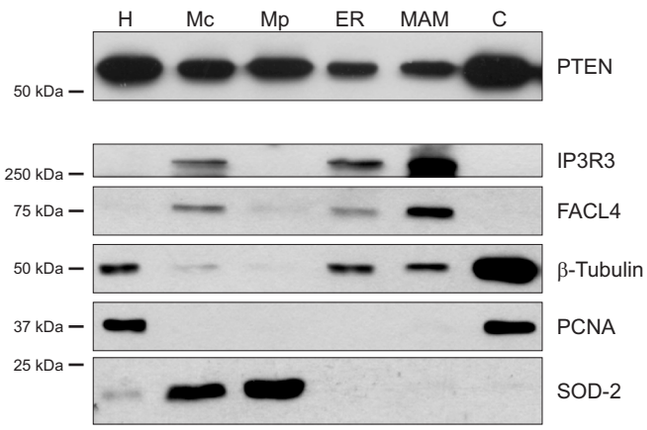

Supplementary Figure 1

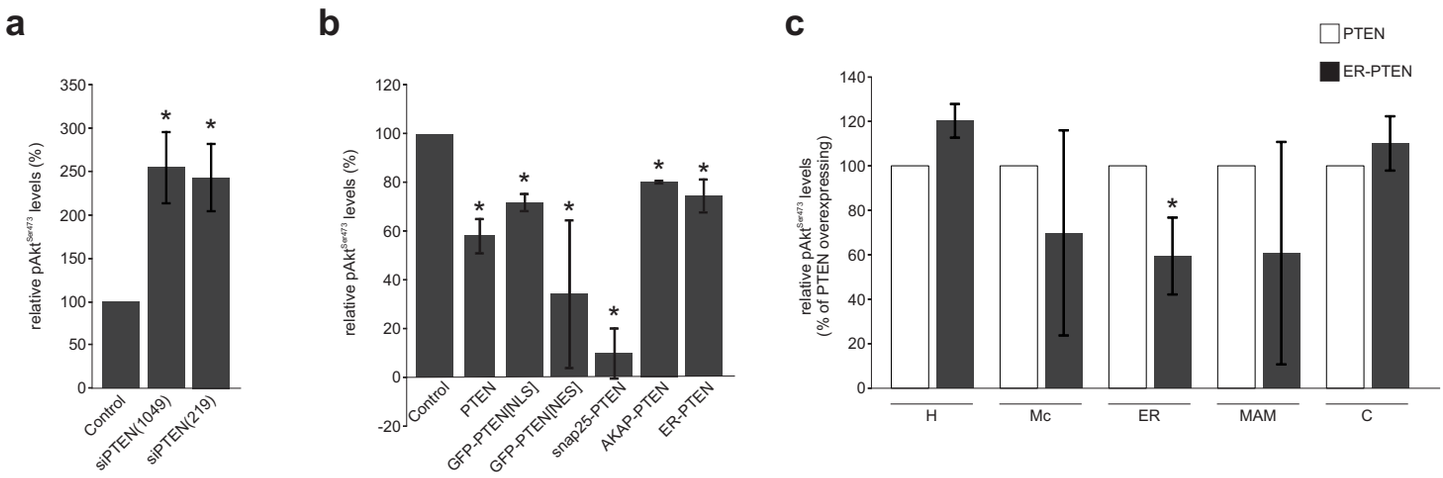

Supplementary Figure 2

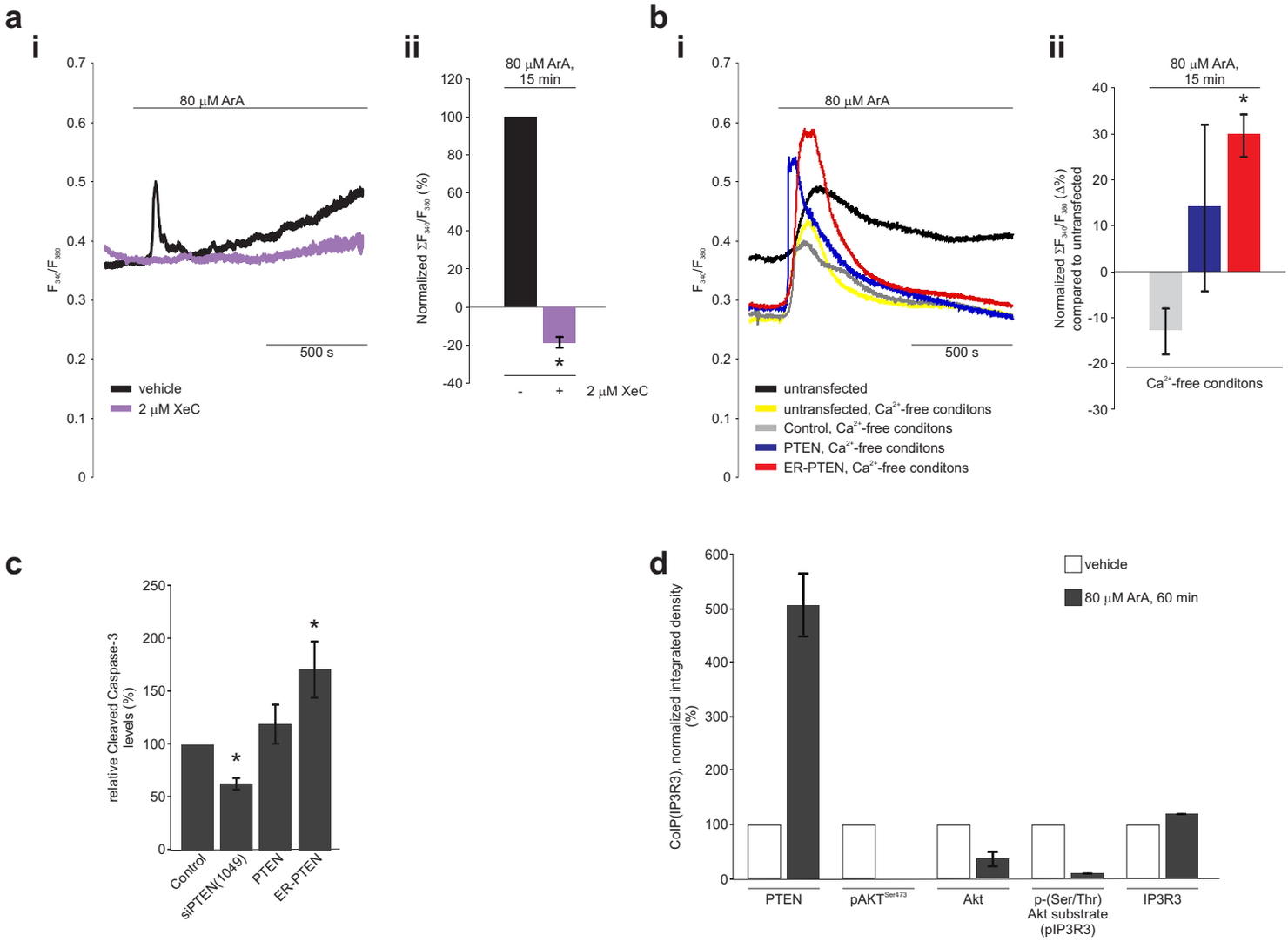

Supplementary Figure 3

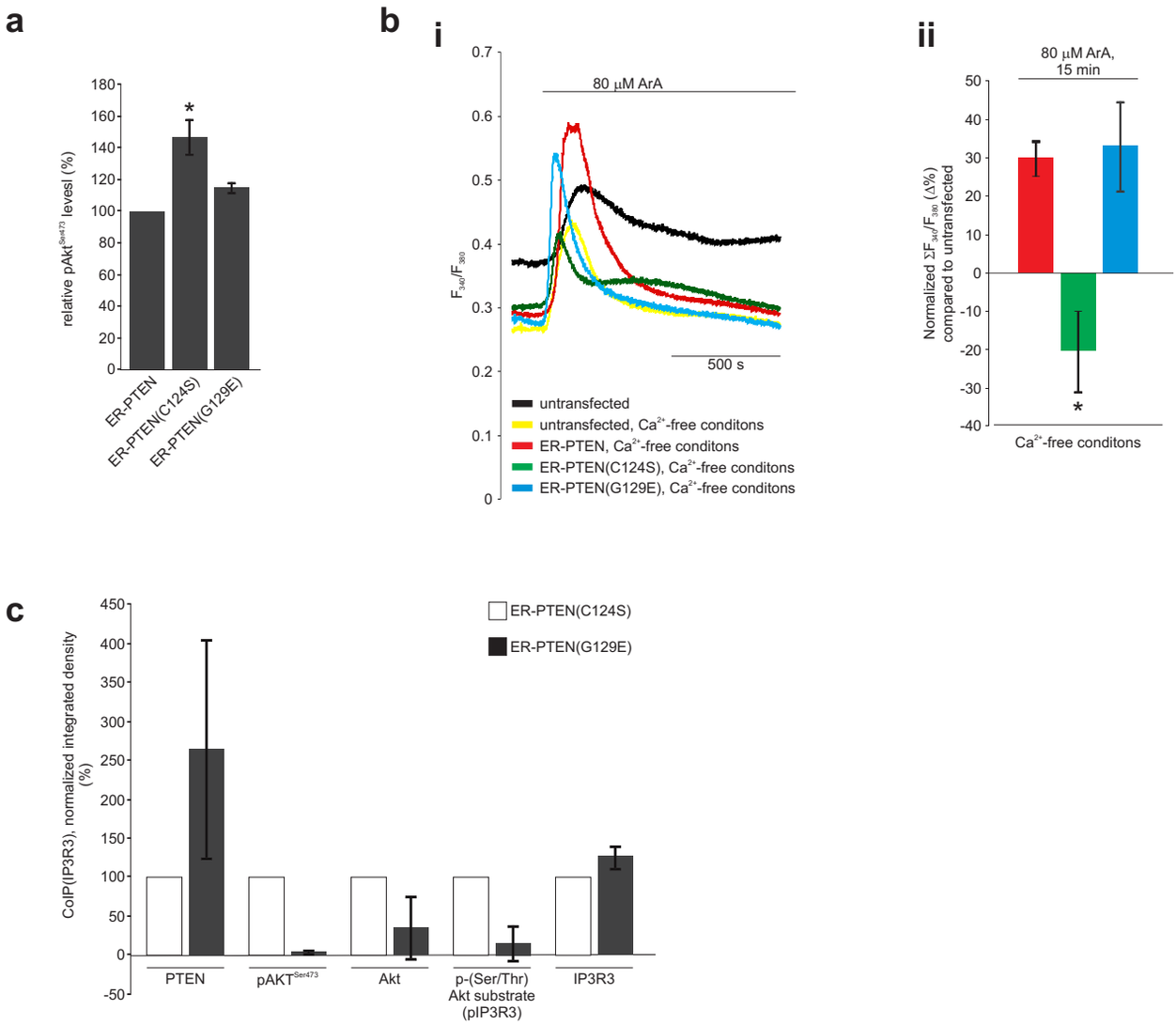

Supplementary Figure 4